GERMAN - MONGOLIAN INSTITUTE FOR RESOURCES AND TECHNOLOGY

The present work was submitted to
the Faculty of Mechanical and Electrical Engineering

NUMERICAL ANALYSIS OF HEAT TRANSFER AND THERMAL EFFICIENCY IN A TRADITIONAL MONGOLIAN GER: INFLUENCE OF CHIMNEY GEOMETRY

Bachelor's Thesis

By

OYUNJARGAL Molomjamts

Study program: Mechatronics Engineering
Student ID: B2200464

1st Supervisor/Examiner: Sungchil Lee, Ph.D, P.E
2nd Supervisor/Examiner: Kim Young Suk, Ph.D

Ulaanbaatar/Nalaikh
2026

Statutory Declaration

Molomjamts, Oyunjargal	B2200464
Last Name, First Name	Student ID Number

I hereby affirm in lieu of an oath that I provided the submitted bachelor thesis

NUMERICAL ANALYSIS OF HEAT TRANSFER AND THERMAL EFFICIENCY IN A TRADITIONAL MONGOLIAN GER: INFLUENCE OF CHIMNEY GEOMETRY

I did not use any sources other than those stated. In case that the work is additionally submitted on a data medium, I declare that the written and the electronic form are completely identical. The work was not submitted in the same or similar form to any examination authority.

Ulaanbaatar/Mongolia, 05.01.2026	
Place, Date	Signature

Acknowledgement

In this section, I express my gratitude and acknowledgement to those who have helped making this thesis come to life. Research of any topic would be incomplete without the existing investigation from previous curious minds on the same topic. I thank every researcher, mentioned in this thesis or not, who put their time and effort into the realm of Mongolian ger and its characteristics.

My deepest gratitude goes to my supervisors, Professor Kim Young Suk and Professor Sungchil Lee, who make time for meetings and gave important insights throughout my research. Their genuine interest on the topic pushed me to do even beyond what I initially anticipated. I would like to also extend my gratitude to Mr. Sergey Zambalov who helped me make sense of the software program I used for the first time while not knowing who I was.

I would like to also show appreciation to my family and friends who allowed me to focus purely on the most important part of my bachelor's degree. To my parents and friends, Aisulu, Khuslen and Uyanga, I deeply appreciated your help on every step of the way.

Lastly, I would like to acknowledge that some AI help was used in this thesis though not prominently; two main uses were navigating through the software used and making the structure of sentences easy to read and not repetitive after drafting the thesis with my own words.

Abstract

This thesis presents a comparative computational fluid dynamics (CFD) investigation into the heat transfer performance of chimney geometries used in Mongolian traditional ger (yurt) heating systems. Using ANSYS Fluent 25 with a two-dimensional axisymmetric transient model incorporating the SST k-ω turbulence model and the Discrete Ordinates radiation model, ten simulation cases were conducted across three categories of geometric variation: chimney inner diameter (0.08 m to 0.12 m), number of external horizontal annular fins (5, 7, and 9), and coaxial cylindrical extension (0.2 m and 0.25 m). The model was validated against experimental field measurements of a coal-heated ger reported by Purev et al. (1) in 2022, achieving agreement within 0.79% at the reference monitoring point. Results for the diameter variation indicate a irregular relationship between chimney diameter and indoor temperature, with a minimum observed at 0.10 m and recovery at 0.12 m due to recirculation effects and increased stove radiation. Chimney wall heat flux increased consistently with diameter, while draft velocity decreased. For the annular fin configurations, contrary to classical fin theory, all finned cases reduced total heat transfer by approximately 60% relative to the bare cylinder baseline. This is attributed to the perpendicular orientation of horizontal fins obstructing buoyancy-driven natural convection and suppressing internal draft through a coupled thermal-fluid feedback mechanism. For the coaxial cylindrical extension, the 0.2 m diameter extension achieved a 16.9% improvement in total convective heat output over the baseline by adding sufficient dissipating surface area, while the 0.25 m extension reduced output by 29.0% due to excessive draft suppression. These results provide the first geometry-based numerical design investigation for ger chimneys, suggesting that the current MASM standard diameter of 0.10 m is thermally suboptimal (though, at the same time it could be the best configuration in the context of quality of indoor air) and that a well-sized coaxial extension represents the most promising configuration for enhancing ger heating efficiency.

Table of Contents

Acknowledgement i
Abstract ii
1 Introduction 1
1.1 Background 1
1.2 Research Motivation: The Gap in Chimney Research 1
1.3 Research Objectives and Questions 3
2 Literature review 5
2.1 Effect of Chimney figure on Heat Transfer 5
2.2 Heat Transfer Mechanisms 6
2.3 Influence of Chimney Diameter on Heat Transfer and Draft 7
2.4 Effect of Chimney Surface Modifications on Heat Transfer 8
2.4.1 Annular fin configuration 8
2.4.2 Coaxial cylindrical extension 9
3 Methodology 11
3.1 Finite Element Model for Analysis 11
3.1.1 Turbulence Model: SST k-ω 11
3.1.2 Radiation Model: Discrete Ordinates (DO) 12
3.1.3 Modelling approach 13
3.2 FE Model Assumptions and Boundary Conditions 13
3.3 Model Configuration 16
3.4 FE Model Validation 17
3.4.1 Verification against reference 17
3.4.2 Convergence validation 19
3.4.3 Mesh validation 20
4 Result and Discussion 22
4.1 Data collection 22
4.2 Influence of Varying Diameter 23
4.2.1 Flow velocity 23
4.2.2 Temperature on monitor points 24
4.2.3 Radiation heat flux from the stove surface 25
4.2.4 Chimney wall heat flux 26
4.3 Influence of Varying Number of Annular Fins 27
4.2.1 Total Surface Heat Flux and Heat Transfer Rate 27
4.2.2 Chimney Wall Temperature and Draft Suppression 29

4.2.3 Monitor Point Temperatures and Internal Gas Behavior 30
4.2.4 Stove Surface Heat Flux Response 31
4.3 Influence of Coaxial cylindrical extension 32
4.3.1 Total heat transfer derivation from surface area 32
4.3.2 Chimney wall temperature 33
4.3.3 Stove Total Surface Heat Flux 34
4.4 Comparison between annular fin variation and cylindrical extension variation 35
5 Limitations 36
6 Conclusion 37
7 References 39
APPENDIX A: List of Tables, Figures and Equations 41
APPENDIX B: Designs used for the cases of annular fins and cylindrical extension 42
APPENDIX C: Data collected from simulation results 43
APPENDIX D: Temperature against time graph for the two monitor points at specified diameter of chimney (Diameter variation case) 44

1 Introduction

1.1 Background

The Mongolian Traditional Ger, with a history spanning thousands of years (2), is a portable structure with round walls connected to the crown (*toono*) by roof rafters (*uni*), and its unique roof design sets it apart from other round houses (3). It is suitable for lifestyles of nomadic people in any weather; In the summer heat, a vertical-driven vortex, induced by the opening at the crown, effectively gets the cooler air circulating when properly ventilated and in the harsh winter, multiple coverings on the roof, mainly felt made by sheep wool, are added to reduce heat loss and keep “thermal comfort” (4). Once heated, it is a reliable form of housing in the cold months; however, problems arise in getting it heated. As of 2019, approximately 200,000 households, 40% of them living in *gers*, burn raw or processed coal/upgraded briquette fuels in small household stoves for warmth day and night (5). When this is taking place in the world’s coldest capital city, health, environmental and other problems get inevitable as time progresses.

In the urban setting, most of the *gers* rely on a small individual coal- or wood-burning stove for all space heating. The stove is connected to a simple steel chimney that exits through the *toono* at the apex of the roof. The geometry of this chimney, its diameter, height, and surface configuration, directly determines how efficiently combustion heat is transferred from the flue gases to the indoor space (6) and how effectively draft is maintained to sustain clean combustion. Chae et al. (6) concluded in their research, there is an optimal diameter for chimneys as higher or lower than that optimal amount would result in ineffective heat removal, leading to the chimney’s thermal performance to be poor. In recent years, the number of research papers published on *ger,* and its heating system’s thermal characteristics is increasing due to several reasons, one of them being the byproducts from stove’s fuel combustion causing health risks like carbon monoxide (CO) poisoning (7), other pulmonary and cardiovascular issues (8).

1.2 Research Motivation: The Gap in Chimney Research

A growing body of work has investigated the thermal behavior of the *ger* from several directions, yet the chimney system has been consistently treated as a fixed boundary condition rather than as an object of optimization.

Experimental studies on *ger*, specifically ger insulation, have shown that adding thermal mass to the envelope significantly reduces heat loss: the indoor comfort level and energy

efficiency of a *ger* with added insulation and an electric thermal storage heater were shown to be enhanced compared with those of a reference *ger* with standard envelope materials (5). Research on heating system alternatives has evaluated electric thermal storage heaters, solar photovoltaic systems, and solar thermal collectors as replacements for the coal stove, motivated primarily by the need to reduce the severe air pollution produced by solid-fuel combustion in the ger districts (9). In another study, Du et al. evaluated multiple retrofitting strategies, three types of electric heating systems, and photovoltaic integration (10). Multiple people have also carried out field measurements of varying duration with the focus being *ger* itself. Purev and Hagishima (1) collected temperature data of 2 *gers* over 10 days for coal-burning stoves and 2 extra days for an electric heater. A broader measurement was done by UNICEF Mongolia's Ger of the 21st Century project (11), where 183 ger in *Bayankhongor*, Mongolia was monitored for 2019-2020 winter months.

Thermal simulations of the *ger* interior have also been carried out. Research using dynamic calculation tools has aimed to create a database of the energy and climate comfort qualities of traditional *gers* and to develop improved building prototypes based on yurt experiments. More recently, a three-dimensional numerical simulation of carbon monoxide distribution inside a *ger* using COMSOL Multiphysics showed that indoor CO concentration near the stove and *ger* center can reach levels three times higher than the WHO recommended indoor guideline of 6 ppm, with the distribution pattern strongly governed by the chimney's sealing integrity and the stove operating conditions (7). B.Battsetseg et al. also researched how an array of vertical tube enhancements placed in the rear section of the stove could influence its performance using numerical simulations (12).

What is lacking in all this work is any systematic investigation of the chimney itself as a heat transfer component. There is a study for electrostatic dust precipitator (ESP) (8) which is a specialised residential technology for coal and wood-fired stoves that utilises high-voltage power (13–30 kV) to charge and capture fine particles from exhaust plumes. It functions by collecting up to 99.5% of fly ash and particulate matter, effectively preventing the release of toxic trace elements into the atmosphere and the wider environment. This simple yet sophisticated system is a chimney enhancement in a way; however, the researchers didn’t account for its thermal effects on the surroundings. The chimney diameter, the presence or absence of fins on its outer surface, and the possibility of adding a coaxial outer cylinder to create an annular flow passage have never been studied numerically or experimentally in the context of the *ger.* This is a

meaningful gap, because the chimney is simultaneously the main pathway for heat loss from the stove to the indoor environment, the driver of natural convection draft that sustains combustion, and the component most directly responsible for the quality of indoor air (11,7).

This gap is further sharpened by a practical challenge. The Mongolian Agency for Standards and Metrology (MASM) has established some technical standards, listed in table 1, for *ger* stove and chimney dimensions (13), but the origins of these standards are hard to find. It is therefore meaningful to carry some suspicions around the topic and question whether it is the optimal dimensions that are set as the standard.

Table 1. Technical standards by MASM (13)

Stove	**Parameter**	**Chimney**	**Parameter**
Thickness	0.002m	Diameter	0.1m
Power	3-15kW		
Efficiency	70%		

1.3 Research Objectives and Questions

This thesis addresses the identified gap by performing a comparative numerical analysis of heat transfer and thermal efficiency for *ger* chimneys across a range of geometries. The primary configurations studied are as follows: a bare cylindrical chimney at five inner diameters of 0.08 m to 0.12 m; the same chimney fitted with horizontal fins (5,7,9); and a chimney enclosed within a coaxial outer cylinder, inspired by the ESP geometry (8). A total of ten CFD simulation cases are used to derive comparative conclusions about how chimney geometry influences the temperature distribution, heat transfer rate, and overall thermal efficiency of the *ger* heating system. The specific research questions are as follows:

1. How does varying the chimney inner diameter between 0.08 m and 0.12 m affect the natural convection heat transfer and draft performance of the chimney?
2. Do horizontal fins on the chimney outer surface improve thermal efficiency compared to the bare cylinder, and if so or if not, which fin parameter affects the heat transfer for the better the most?
3. Does a coaxial cylindrical extension enhance or reduce chimney thermal efficiency relative to the bare configuration?
4. Which of the configurations studied best satisfies the combined requirements of high heat transfer to the indoor space and sufficient draft for clean combustion?

The answers to these questions are expected to provide the first geometry-based design recommendations for *ger* chimneys grounded in numerical heat transfer analysis.

2 Literature review

2.1 Effect of Chimney figure on Heat Transfer

Ger's heating system is made of a stove, where the heat generation is, and a chimney, through which the exhaust gases are released into the atmosphere. A chimney's operating principle was defined as early as 1899: a column of hot gas is less dense than the surrounding cold air, and this density difference produces a pressure imbalance that drives flow upward through the chimney and draws fresh air in from below (14). This is the phenomenon of natural draft, and its theoretical foundation lies in the classical treatment of buoyancy-induced flows in vertical channels (15).

Today, the stove has been researched from many different angles in the context of *ger*. However, the same could not be said about chimneys as they are generally simplified into being one with the stove (7) or it gets disregarded entirely. If not confined only to the *ger* aspect, the effects of chimney's geometry and thermodynamics properties on efficiency and other parameters have been getting attention as early as 1942 (16).

In 1942, Elenbaas (16) conducted one of the earliest systematic analytical and experimental investigations into heat dissipation by free convection from the inner surfaces of vertical tubes with varying cross-sectional shapes; including circular, rectangular (aspect ratios of 1:1, 1:2, and 1:5), and equilateral triangular geometries. A key practical finding is that an optimal hydraulic radius exists for each cross-section shape that maximizes heat dissipation per unit of cross-sectional area, and at this optimal radius the heat dissipation per unit surface area is essentially independent of cross-sectional shape. Among the shapes studied, the equilateral triangle offers marginally superior volumetric performance due to its lower ψRe value (which is a dimensionless shape factor which indicates how easily a fluid flows through a channel of a given cross-sectional geometry under a pressure gradient), while the square cross-section dissipates approximately 19% more heat than parallel plates at their respective optimal spacings.

In another study, Haaland et al. (17) concluded that the specific distribution of a heat source at the inlet of a vertical channel, whether a discrete horizontal line source (channel plume) or a uniformly distributed source (parallel-walled chimney), significantly affects performance in short and wide channels but becomes irrelevant in tall and narrow channels. For short, wide channels, a uniformly distributed source induces a larger mass flow than a line source of equal strength, while the line source produces a greater bulk temperature rise and a velocity profile that is more highly peaked at the centerline. In

contrast, for tall and narrow channels, the induced flows and temperature rise for both source types are identical and are well-approximated by a fully developed flow model. Furthermore, the researchers observed that in wider channels, the results for a channel plume align closely with those of a classical free plume because the plume does not span the entire width of the channel, allowing for fluid entrainment similar to that in an unbounded environment.

More recently in 2015, Chae et al. (6) investigated the enhancement of buoyancy-driven heat transfer in chimney systems through a combination of numerical CFD simulations and mass transfer experiments based on analogy concepts. The study concludes that increasing the height of a chimney consistently enhances heat transfer rates for all Prandtl numbers because a taller chimney extends the working distance of the buoyancy force, thereby increasing the fluid flow rate. Crucially, the researchers identified an optimal chimney diameter that maximizes heat transfer efficiency; they observed that while large diameters result in weak boundary layer interactions and a smaller chimney effect, excessively small diameters create high friction that impairs heat removal.

2.2 Heat Transfer Mechanisms

The heat transfer from the outer surface of a chimney to the indoor space of a *ger* occurs through three mechanisms simultaneously: natural convection of indoor air across the chimney surface, thermal radiation from the hot chimney wall to surrounding surfaces, and conduction through the chimney wall itself (18). In practice, for a steel chimney operating at several hundred degrees Celsius, radiation and natural convection are of comparable magnitude, and neither can be neglected.

Natural convection from the outer surface of a vertical cylinder is one of the classical problems in heat transfer. When the diameter of the cylinder is large relative to the thickness of the developing thermal boundary layer, the flow behavior and heat transfer correlations approach those of a vertical flat plate, and the Nusselt number scales as $\mathrm{Nu} = 0.67\mathrm{Ra}^{0.25}$ in the laminar regime ($Gr < 10^9$) (19,18). This asymptotic behavior is well established both experimentally and numerically. As the cylinder diameter decreases relative to the boundary layer thickness, curvature effects become important, and the Nusselt number for the cylinder exceeds that of the flat plate for the same Rayleigh number — a result attributed to the thinning of the boundary layer on the convex surface.

Radiation from the chimney surface plays an equally important role. The Stefan-Boltzmann law gives the net radiative heat flux from a surface at temperature T_s to a surrounding enclosure at temperature T_∞ as

Equation 1

$$q_{rad} = \varepsilon\sigma({T_s}^4 - {T_\infty}^4)$$

, where ε is the surface emissivity and σ is the Stefan-Boltzmann constant (18,20).The contribution of radiation through the stove in *ger* was approximated by Purev et al. (1) in their research and it was around 70% - 77% of total heat generated. The conjugate nature of the problem is sometimes not considered in numerical studies (21). For the *ger* chimney, this conjugate character is important because the steel wall has finite conductivity and thickness, and the relative magnitude of inner-surface convection, wall conduction, and outer-surface radiation and convection all influence how much heat is delivered to the indoor space versus lost to the atmosphere above the toono.

The Boussinesq approximation is used in this thesis and it is the standard simplification used in numerical chimney studies, treating the fluid density as constant except in the buoyancy term of the momentum equation. Numerical simulations of natural convection heat transfer and fluid flow use the Boussinesq approximation to account for the buoyancy effect, which treats fluid density as invariant except in the body force term of the momentum equation (22,23,21). This approximation is valid when the temperature difference between the wall and the fluid is small relative to the absolute temperature, a condition that is approximately satisfied for the outer surface of the *ger* chimney. CFD studies of chimney flows almost universally adopt this approximation, and doing so simplifies the governing equations to the incompressible Navier-Stokes equations with a temperature-dependent body force term, solved alongside the energy equation.

2.3 Influence of Chimney Diameter on Heat Transfer and Draft

The diameter of a chimney is among its most consequential geometric parameters, with effects that operate simultaneously on the draft, the internal flow regime, the boundary layer development, and the heat transfer from the outer surface. These effects are not monotonic — there are competing mechanisms that produce an optimal diameter for maximizing specific performance metrics — making the choice of chimney diameter a genuine engineering design problem rather than simple optimization. Other than the research done by Haaland et al., there are multiple papers that support this claim.
Ohk et al. (22) studied the transition of fully developed regime to a developing flow regime systematically in open vertical pipes, varying the diameter from 3 mm to 30 mm for pipe lengths of 0.2–1.0 m and Prandtl numbers from 0.7 to 2,014. For large-diameter pipes

or high-Prandtl-number fluids, the thermal boundary layers on opposite walls do not interact, and heat transfer matches the vertical plate correlation. As the diameter is reduced, boundary layers merge and two distinct secondary behaviours emerge depending on the Prandtl number; in short, the heat transfer to the ambient air is impaired as the diameter is decreased.

Later, Kang et al. (23) complemented this with a more detailed investigation at a very high Prandtl number (Sc = Pr = 2094), identifying three distinct heat transfer regimes as a function of cylinder diameter at fixed height. At very small diameters (below ~7 mm), heat transfer deteriorated by up to 31% below the vertical plate correlation because flow stagnated at the cylinder base under the combined effect of overlapping boundary layers and high viscous resistance. At intermediate diameters (~9–15 mm), the chimney effect enhanced heat transfer above the vertical plate baseline by increasing the mass flow rate into the cylinder inlet through an internal plume acceleration mechanism. At large diameters (above ~20 mm), boundary layers were too thin to interact and duct flow conditions prevailed with heat transfer returning to the vertical plate correlation. These three regimes reflect fundamentally different fluid dynamics inside the cylinder, with the intermediate chimney-effect regime being most relevant to practical chimney design for maximizing heat extraction from the flue gas.

2.4 Effect of Chimney Surface Modifications on Heat Transfer

Beyond the bare cylindrical chimney, two main categories of geometric modification can be made to enhance the heat transfer from it: the addition of extended surfaces in the form of fins, and the installation of a second wall around the chimney, forming concentric cylinders

2.4.1 Annular fin configuration

Fins are protruding, extended surfaces on an arbitrary shape or device that needs cooling. Depending on factors such as manufacturing cost, the weight it adds and its influence on the heat transfer coefficient and flow, the fin design is created. This optimization is widely used on electronic devices such as power transistors and computer video cards in relevance to the overheating of them would cause the whole system to break down (20). Q. Shen et al. (24) compared how varying number of longitudinal fins (See Figure 1a for reference) and its height would affect the heat transfer properties and implicitly compared it to bare cylinder. They concluded that increasing the number of fins leads to less fluctuation of thermal boundary layer which gives better heat transfer rate; All 6 variations tested outperformed bare cylinder heat transfer as in essence, fins

increase the surface area through which heat is given off, leading to enhancement of Nusselt number (20).

Looking beyond the use, the general shape, cylinder with fins, has also been studied. For example, J.R Senapati et al. (25) modelled the following design, Figure 1b, using FLUENT 15 and varied multiple different parameters like Rayleigh number, fin to tube diameter ratio and fin spacing to tube diameter ratio. The most important finding in this research is that bare cylinder's total heat transfer is notably lower (about 4 times) than finned cylinder with a fin to tube diameter ratio of 5 in any turbulence model used. Similarly, E. Hahne et al. (26) and Park et al. (27) researched this topic and got the result that finned surfaces extrude more heat than bare surfaces.

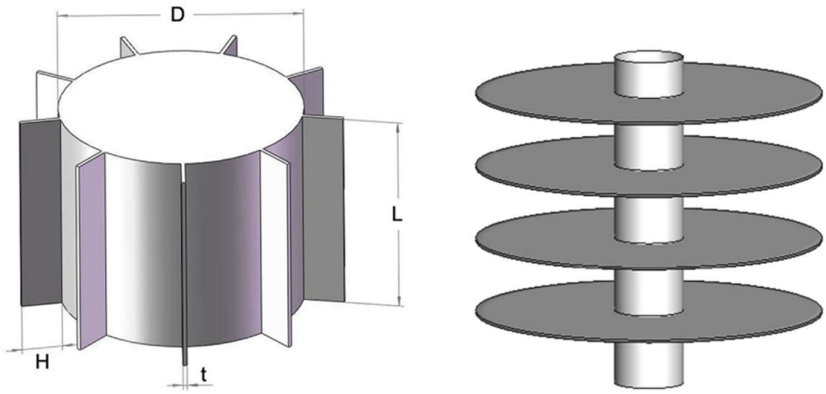


Figure 1. a) Vertical cylinder with longitudinal fins designed by Q. Shen et al. (24) b) Vertical cylinder with annular fins designed by J.R Senapati et al. (25)

2.4.2 Coaxial cylindrical extension

The inspiration to investigate this geometrical configuration came from the electrostatic dust precipitator (ESP) developed for *ger* stoves by Stehr et al. (8). The ESP, which was tested on 70 household stoves in Ulaanbaatar's Bayankhoshuu district over the 2018–2019 heating season, consists of a 200 mm or 250 mm diameter outer cylindrical tube mounted coaxially below the standard chimney pipe, with high-voltage electrodes inside the annular space that charge and collect fly ash particles (See Fig. 2).

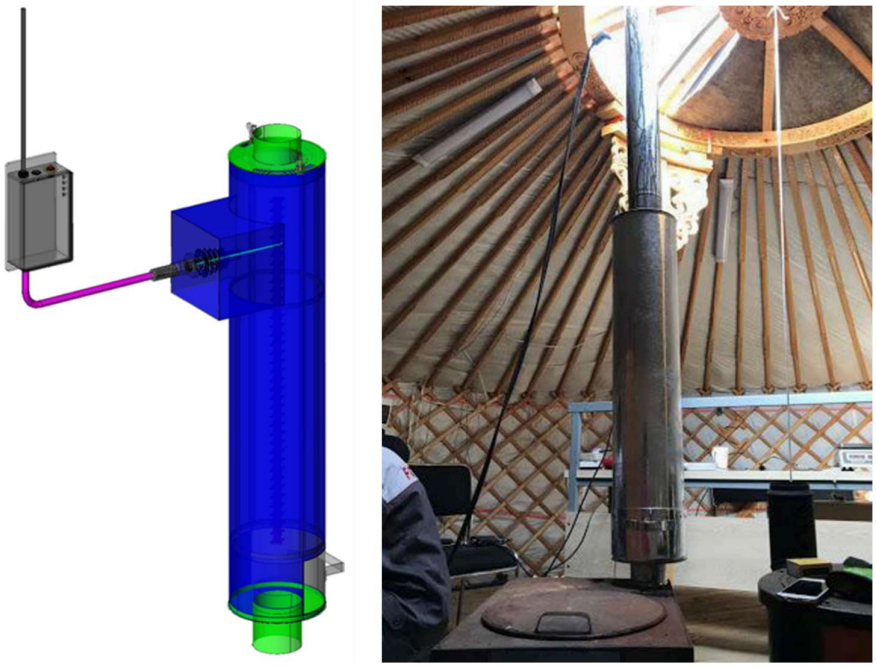


Figure 2. ESP system's design and state after installation by Stehr et al. (8)

Stehr et al. reported PM10 collection efficiencies of up to 60% with raw coal and up to 82% with improved briquettes, and the field test confirmed that the device could be reliably installed and operated in real *ger* conditions through a Mongolian winter. The thermal performance of this annular geometry, however (how much additional heat is transferred to the room by the outer cylinder relative to the bare inner chimney) has not been characterized. This thesis addresses this gap by treating the ESP coaxial geometry as a heat transfer configuration and quantifying its thermal performance relative to the bare chimney and fin-based alternatives.

3 Methodology

3.1 Finite Element Model for Analysis

The numerical simulations in this study were performed using ANSYS Fluent 25, a commercial computational fluid dynamics (CFD) software package widely used in engineering research and industry. ANSYS Fluent solves the governing equations of fluid flow, heat transfer, and radiation using the finite volume method (FVM), which discretizes the computational domain into a finite number of control volumes and enforces conservation of mass, momentum, and energy over each cell (28).

The geometry of the *ger* model was constructed using ANSYS DesignModeler, the integrated geometry-modeling environment within the ANSYS Workbench platform. DesignModeler allows intuitive 2D modelling and editing after shape generation. (28)

3.1.1 Turbulence Model: SST k-ω

To model turbulent convective heat transfer, the Shear Stress Transport (SST) k-ω turbulence model was employed. This two-equation model combines the advantages of the k-ε model in the free-stream region with the robustness of the k-ω model in the near-wall region, making it particularly well suited for flows involving adverse pressure gradients and separated flows. (28)

The model solves two transport equations — one for the turbulent kinetic energy k and one for the specific dissipation rate ω (28):

Turbulent kinetic energy (k):

Equation 2

$$\frac{\partial(\rho k)}{\partial t} + \frac{\partial(\rho k u_i)}{\partial x_i} = \frac{\partial}{\partial x_j}\left[\left(\mu + \frac{\mu_t}{\sigma_k}\right)\frac{\partial k}{\partial x_j}\right] + G_k - Y_k$$

Specific dissipation rate (ω):

Equation 3

$$\frac{\partial(\rho \omega)}{\partial t} + \frac{\partial(\rho \omega u_i)}{\partial x_i} = \frac{\partial}{\partial x_j}\left[\left(\mu + \frac{\mu_t}{\sigma_\omega}\right)\frac{\partial \omega}{\partial x_j}\right] + G_\omega - Y_\omega + D_\omega$$

where G_k and G_ω represent the generation of turbulent kinetic energy and the generation of *ω*, respectively; Y_k and Y_ω represent their respective dissipation terms; D_ω is the cross-diffusion term; μ_t is the turbulent viscosity; and σ_k, σ_ω are the turbulent Prandtl numbers for *k* and *ω* (28).

The turbulent viscosity is computed as:

Equation 4

$$\mu_t = \frac{\rho k}{\omega} \cdot \frac{1}{max\left(\frac{1}{\alpha^*}, \frac{SF_2}{a_1 \omega}\right)}$$

where S is the magnitude of the mean rate-of-strain tensor and $F_2$is a blending function that restricts the limiter to the wall boundary layer (28).

3.1.2 Radiation Model: Discrete Ordinates (DO)

Thermal radiation was modeled using the Discrete Ordinates (DO) radiation model. The DO model solves the radiative transfer equation (RTE) for a finite number of discrete solid angles; each associated with a direction vector fixed in the global Cartesian coordinate system. This approach allows the model to span a wide range of optical thicknesses and can account for radiation in semi-transparent media, scattering, and specular or diffuse wall boundaries (28).

The radiative transfer equation solved by the DO model is:

Equation 5

$$\nabla \cdot (I(\vec{r}, \vec{s})\vec{s}) + (a + \sigma_s) I(\vec{r}, \vec{s}) = an^2 \frac{\sigma T^4}{\pi} + \frac{\sigma_s}{4\pi} \int_0^{4\pi} I(\vec{r}, \vec{s}') \Phi(\vec{s} \cdot \vec{s}') d\Omega'$$

where:

- $I(\vec{r}, \vec{s})$ - radiation intensity at position $\vec{r}$in direction $\vec{s}$
- a - absorption coefficient
- σ_s - scattering coefficient
- n - refractive index of the medium
- σ - Stefan–Boltzmann constant (5.67×10^{-8} W m^{-2}K^{-4})
- T - local temperature
- Φ - phase function for scattering
- Ω' - solid angle

The DO model is particularly appropriate for this study as it captures both surface-to-surface radiation exchange and the participation of interior gas volumes, which are relevant to the thermal environment inside an enclosed *ger* structure (28).

The energy coupling setting in this model is not enabled under the assumption that majority of fluid region (air inside the living space of the *ger*) is optically thin since clean air does not participate in radiation due to no particle being present in it to emit or absorb radiation. (28)

3.1.3 Modelling approach

The traditional *ger* structure is characterized by a geometry that is approximately rotationally symmetric about its central vertical axis, with a cylindrical wall and a conical roof converging toward the central crown opening. This geometric regularity makes it well suited for a two-dimensional axisymmetric modelling approach.

In the 2D axisymmetric model, the three-dimensional geometry is reduced to a two-dimensional cross-sectional plane that is revolved about the central axis for computations. This significantly reduces the computational cost, as the number of mesh cells and associated degrees of freedom are reduced by several orders of magnitude compared to a full 3D mesh. The axisymmetric formulation allows the governing equations of fluid flow, heat transfer, and radiation to be solved in the radial and axial directions only, while the circumferential symmetry is enforced mathematically. This approach is particularly advantageous in the study for time efficiency as transient simulation is preferred and simplification for easier radiation simulation. (28)

After simulation, the results can be shown in 3D as shown in Figure 3. This is especially helpful when visualizing the results, though not necessary for this thesis.

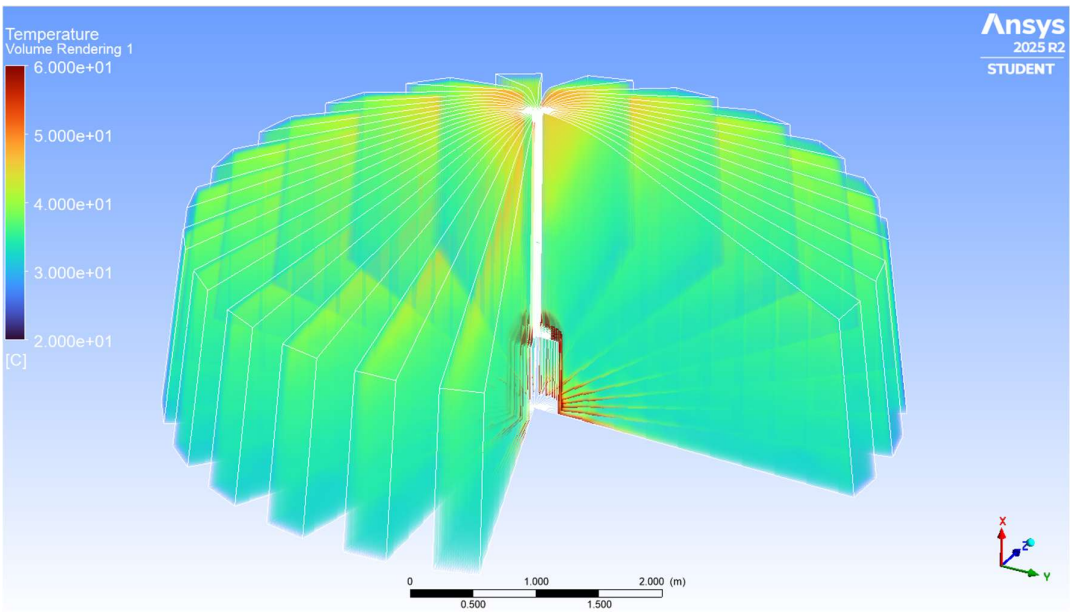


Figure 3. The 2D model result after revolution

3.2 FE Model Assumptions and Boundary Conditions

The following assumptions were adopted in the present numerical study to simplify the computational model while keeping the essential physics of heat transfer within the *ger* interior.

Geometry and Symmetry

As this is a comparative study, 2D models are made under the assumption that asymmetric features like door and non-uniform wool felt envelope are negligible, creating a perfect converging cylinder as the *ger* wall. It is also assumed that the *ger* includes no furniture or any object inside for further simplification. This allows the model to be axisymmetric about the central axis to enable computational efficiency.

Fluid Medium

The interior atmosphere of the *ger* is modeled as a single-phase, compressible Newtonian fluid. The air inside the *ger* is assumed to be slightly participating in radiation due to the presence of light smoke from the central stove and is therefore treated as a weakly absorbing and scattering medium with small but non-zero values of absorption coefficient a. The resulting optical thickness $\tau = (a + \sigma_s)L \ll 1$ confirms that the medium remains in the optically thin regime and that radiative exchange is predominantly surface-driven. To allow natural flow calculations, Boussinesq approximation is adopted.

Stove and Chimney

The stove is modeled as a fluid within solid walls with a prescribed heat generation at the source (fluid) boundary condition. The stove is assumed to ignite at the start of the simulation from a cold initial state, with its wall temperature rising over time as the transient solution develops. The chimney is treated as a cylindrical outlet through which combustion gases escape, and its diameter is varied parametrically across simulation cases.

Transient Conditions

All simulations are performed under transient conditions, capturing the magnitude of temperature and flow fields within the *ger* from an initial cold state toward a thermally developed condition. The initial temperature of the entire fluid domain and all solid surfaces and outdoor ambient temperature are assumed to be uniform, representing the state of the *ger* before the stove is lit. A fixed time step is employed throughout the simulation, and results are recorded at regular time intervals.

Boundary Conditions

The outer surfaces of the *ger* wall and roof are assumed to be subject to constant ambient outdoor temperature conditions. Also, *ger* wall realistically has many layers of wood lattice wall, different types of felt and other insulating material. This sentiment is

simplified to be only wood and heat loss through the *ger* envelope is governed by the heat transfer coefficient and outside temperature which are approximated from the reference study (1). Wind effects and infiltration through the *ger* fabric are neglected in the base model.

Table 2. Boundary conditions for solid parts

Name	Material	Thickness (m)	Heat transfer coef. (W/m^2K)	Emissivity
Ger wall	Wood	0.1	10	0.9
Ger floor	Pure insulator	-	-	0.9
Stove wall	Steel	0.002	N.C*	0.79
Chimney wall	Steel	0.002	N.C*	0.79
Fins	Steel	0.002	N.C*	0.79

N.C* – Numerically calculated

Emissivity values are taken from "Table of Total Emissivity" by Omega Engineering (29). Assuming that majority of inside surface of *ger* wall is covered by wood and emissivity is a property of surface finish generally, value for wood is taken.

Table 3. Boundary conditions for fluids

Name	Material	Density (kg/m^3)	Thermal expansion coefficient (K^{-1})	Abosrption coefficient (m^{-1})	Heat generation
		Boussinesq approximation			
Ger fluid	Air	1.225	0.0033	0.055	-
Stove fluid	"Smoke"			5	$45000 W/m^3$
Chimney fluid	"Smoke"			5	-

As a baseline for validation, values shown in Figure 4. from the experimental study done by U. -U. Purev et al. (1) were taken. Specifically, measurements made of *Ger* B between 9:00 to 10:30 on 18th of January were taken as true on the basis that these numbers reflect a scenario where the *ger* has had enough time to cool down to the same temperature at all points and is heated up continuously; the value for the absorption coefficients of air and smoke were selected by trial-and-error method after failed iterations to simulate the environment closest to the experimental results.

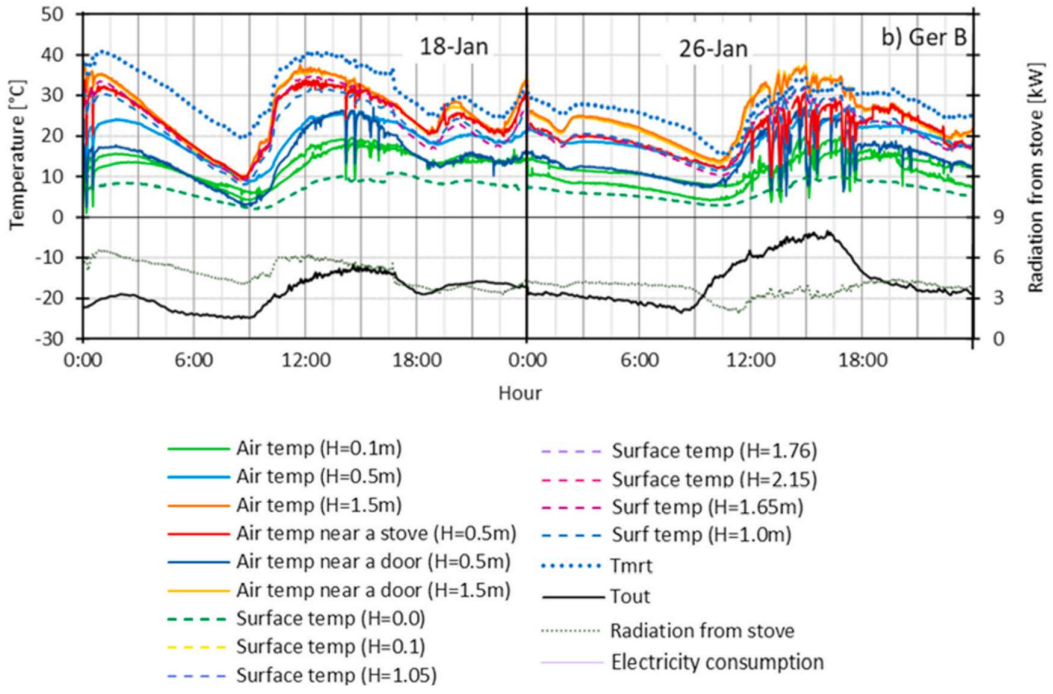


Figure 4. Measurements of ger temperature using coal stove

Also, U. -U. Purev et al. estimated the stove's total power of said *ger* subject to be 6.06kW. From here, simple calculations were made to find the heat generation for stove fluid and rounded down:

$$P_{out} = 6060W * \frac{70\%}{100\%} = 4242W$$

$$V_{stove} = 0.0929m^3*$$

$$q_v = \frac{4242W}{0.0929m^3} = 45662\frac{W}{m^3}$$

*The volume used above is the volume of the cylindrical stove when revolved around the central axis.

These steps of carefully choosing the parameters and matching the result to the experimental study were a crucial one to take as more realistic environment is desired even if this thesis is a comparative research.

3.3 Model Configuration

As the reasoning stated earlier in section 3.2, the main design follows the *ger* dimensions of the experimental study as shown in Figure 5.

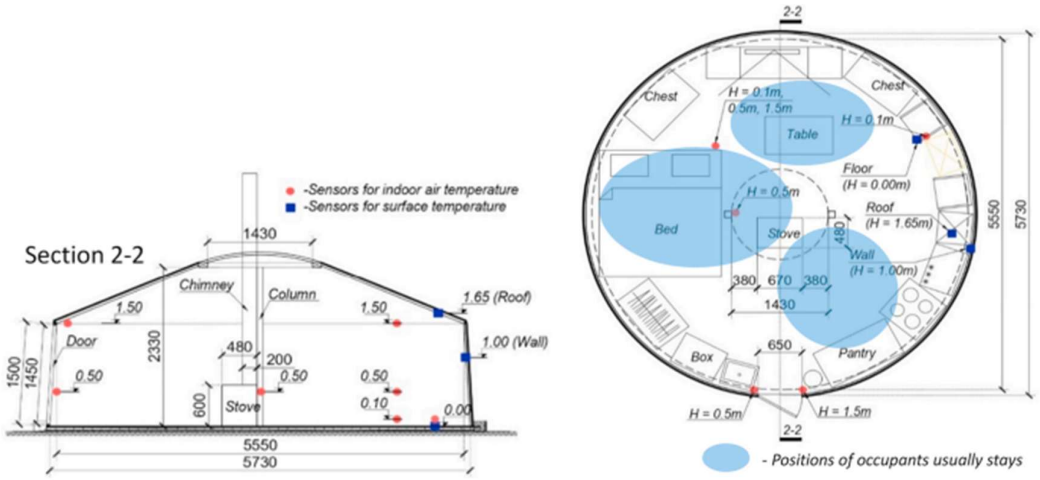


Figure 5. Detailed figure of dimensions by U. -U. Purev et al.

Following figure depicts the base models with chimney diameter of 0.1m on which all other configurations are made.

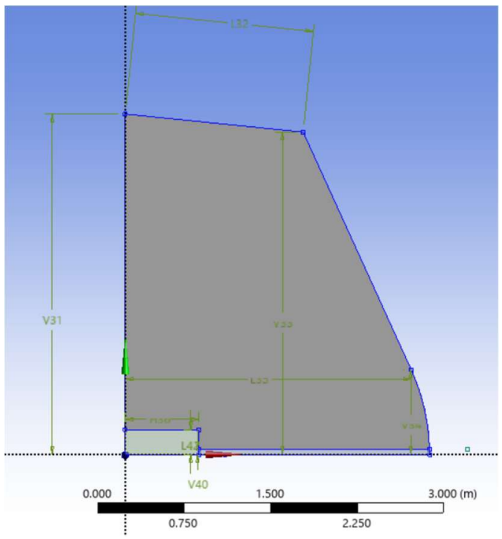


Figure 6. 2D model

Reason for rotation of the 2D model is because the axisymmetric model only allows revolution about the x-axis. To avoid confusion from this point, figures will include the model as rotated and upright.

3.4 FE Model Validation

3.4.1 Verification against reference

First, comparison between simulation and reference was made on one point. As mentioned earlier, measurements done by U. -U. Purev et al. are taken as a reference; a constant of -25˚C for ambient outside temperature, 10˚C for initial ambient inside temperature and 29˚C for reference point (Figure 7).

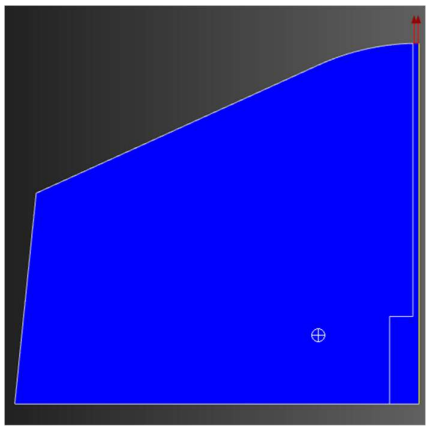


Figure 7. Reference point relative to the ger fluid (locally; x=-0.735m, y=0.5m)

This main comparing point of temperature-near-stove is chosen as other points would include the influence of obstacles or heat loss points placed in the way of fluid flow. Figure 8 depicts the temperature-near-stove plotted against time (5400s or 1.5h) for the standard 0.1m diameter chimney.

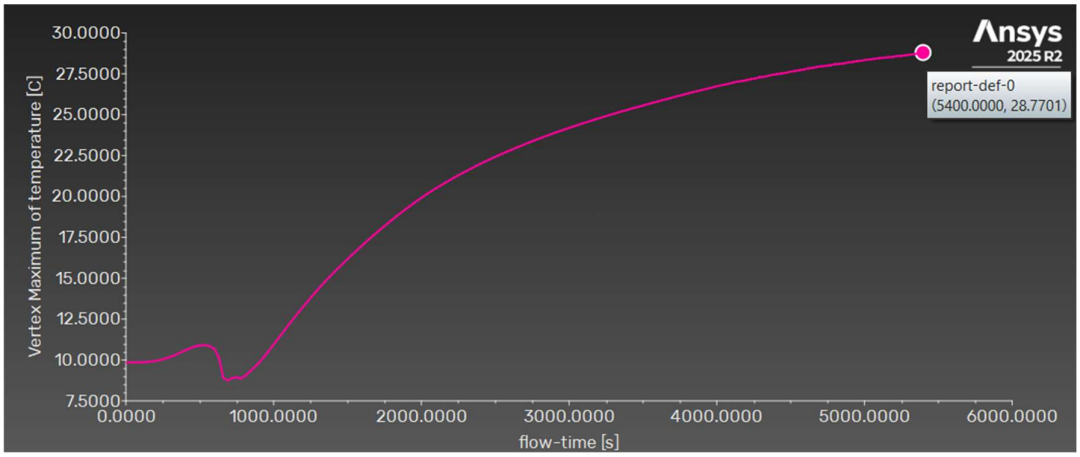
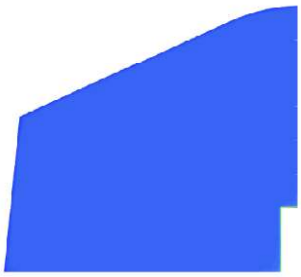
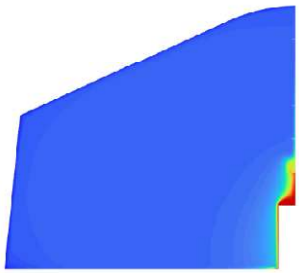
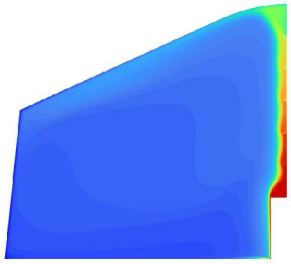
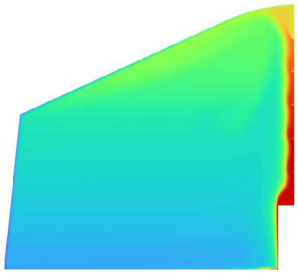
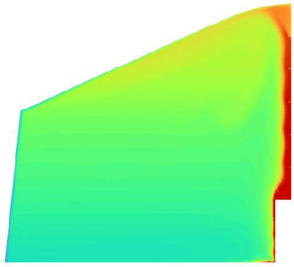
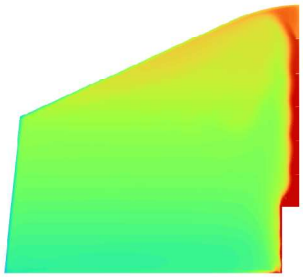


Figure 8. Temperature-near-stove against time graph for chimney d=0.1m

Here, at the 90-minute mark, the point's temperature is 28.7701˚C, which is within 5 percent of difference, specifically 0.79 percent.

Secondly, physical sanity check was done on the contours of the *ger* fluid at each time frame (see Table 4). Heat is dissipated the most from stove first as chimney is not yet heated. Over time, hot air movement is directed towards the central crown opening while cold air coming in through *ger* walls cool down area around *ger* floor. These observations are in line with heat transfer basic knowledge that hot air rises and cold air sinks.

Table 4. Contours of key time frames: an example

t=0min	t=5min	t=10min
		
t=30min	t=60min	t=90min
		

3.4.2 Convergence validation

In a CFD simulation, the governing equations, conservation of mass, momentum, energy, and any additional transport equations, are solved iteratively rather than exactly. At each iteration, the solver computes an approximate solution and substitutes it back into the discretized equations. Because the solution is not yet exact, there will be a remaining imbalance in each equation: this imbalance is the residual. Formally, for a given transport equation, the residual at iteration n is the sum of all the source, flux, and rate-of-change terms evaluated at the current approximate field values. A residual of zero would mean the discrete equations are satisfied exactly, which would only be achieved at true convergence.

In ANSYS Fluent, these imbalances are normalized before being reported. For steady-state problems, normalization is typically performed against the largest absolute residual value encountered during the early iterations, which scales the residual history so that all quantities begin near a value of 1 and decrease as the solution develops. For transient simulations, which is the case in the present study, the residuals are evaluated within each time step and represent how well the iterative inner-loop solver has converged within that single time step before advancing to the next one. The transient residual

therefore resets at each time step rather than monotonically decreasing throughout the entire run.

As all cases have similar boundary conditions (of course chimney diameter/geometry changes) and mesh size, the residuals plots have similar look to them for the entirety of 14400 iterations (80 iterations per time step for 180 iterations). One of the examples' residual plots is shown in Figure 9.

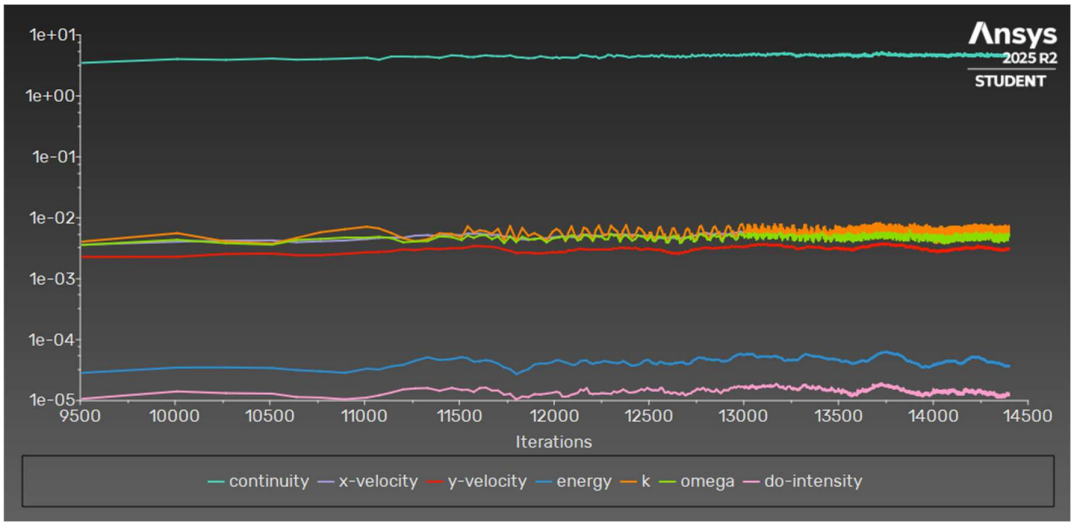


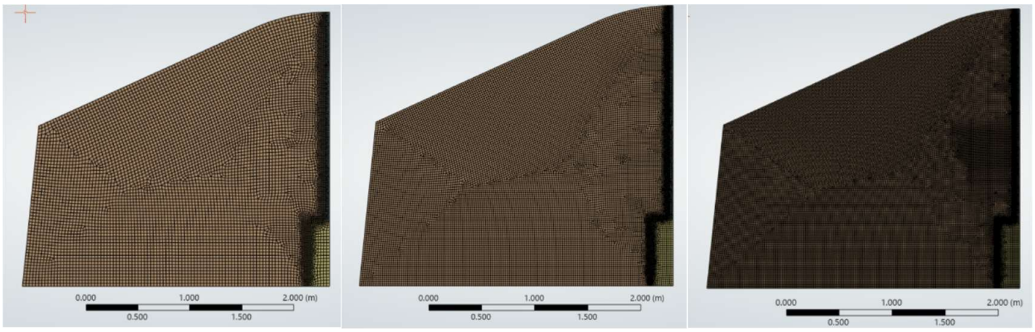
Figure 9. Residual plot example

For the CFD simulations at hand, it is desirable to get each parameter below 2 to 3 orders of magnitude as stated by moderators in ANSYS Fluent Learning Forum (30); however, it is not a law. Everything except the continuity line fulfill this "requirement", making it easier to overlook the continuity problem with other methods of validation and verification mentioned in this section.

Moreover, the example graphs of temperature on monitor points placed at specific coordinates show stabilizing behavior at the end through each case as shown in Appendix D, which further creates assurance.

3.4.3 Mesh validation

For simulation, mesh size and overall quality play a big role in the result. Hence, mesh validation was performed by varying the cell size by 1.5 times (can be seen from Figure 10) and making the baseline mesh, which is used for all simulations, finer each time.



(a) (b) (c)

Figure 10. (a) Coarse mesh (b) Medium mesh (c) Fine mesh used for quality check

Table 5 shows the collected monitor values for each mesh.

Table 5. Values for mesh quality check

	Coarse (base)	Medium	Fine
Cell size (Face/Edge)	0.03/0.01	0.02/0.0067	0.0133/0.0044
Number of elements	9284	19226	41410
Temperature on reference point (˚C)	33.37	34.27 (+2.7%)	34.74 (+4.1%)
Heat flux at *ger* wall	71.39	73.81 (+3.4%)	74.82 (+4.8%)

The temperature and heat flux values for all 3 have differences of less than 5 percent which makes the baseline cell size justified and reasonable.

4 Result and Discussion

4.1 Data collection

Upon completion of each simulation, data was extracted from ANSYS Fluent in a systematic manner to enable consistent comparison across all five cases. The collected outputs fall into two broad categories: spatial field data visualized as contour plots, and surface- or boundary-averaged scalar quantities exported as numerical values.

For the spatial field data, temperature contour plots were captured at each recorded time step throughout the transient simulation. These plots provide a visual account of how the thermal and flow fields develop within the *ger* interior over time, from the initial cold state through to the thermally developed condition. Temperature contours allow the progression of stratification, the extent of the heated zone, and the influence of buoyancy-driven flow to be observed directly. By collecting these plots at consistent time intervals across all simulations, meaningful frame-by-frame comparisons between configurations become possible.

For the boundary-averaged scalar quantities, in general, five metrics were recorded at the end of each simulation on average. Of course, considering different cases require different parameters to be analyzed, number of metrics evaluated are different for each case. Temperature for two different monitor points was recorded for every minute of flow time. Figure 11 shows the axial location of these points relative to *ger* fluid.

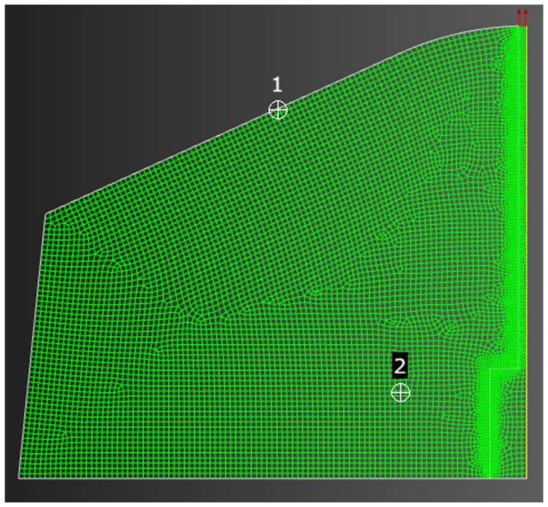


Figure 11. Locations of two monitor points

The area-averaged temperature and fluid velocity at the chimney outlet were extracted to characterize how effectively each configuration drives hot gas out of the *ger*. These two quantities together describe the nature of the chimney draft; a high temperature

combined with a high exit velocity indicates strong buoyancy-driven exhaust, while discrepancies between cases point to differences in how each chimney configuration interacts with the interior flow field. Additionally, the heat flux through both the stove surface and the chimney wall was recorded. The stove heat flux serves as a check on the internal consistency of the energy input across simulations, while the chimney heat flux quantifies how much thermal energy is lost through the exhaust rather than retained within the interior. Together, these scalar outputs provide a concise and quantitatively comparable summary of each simulation's thermal performance, complementing the qualitative picture provided by the contour plots.

4.2 Influence of Varying Diameter

This section goes over the results obtained from the transient CFD simulations of the *ger* model with chimney pipe diameters ranging from 0.08 m to 0.12 m. The key output parameters examined include the monitor point temperatures at two axial locations, mean flow velocity within the chimney, the average chimney wall temperature, heat flux from the stove surface, convective heat flux through the chimney wall, and the radiative heat flux from the stove wall. These values are available in Appendix C, Table C1.

4.2.1 Flow velocity

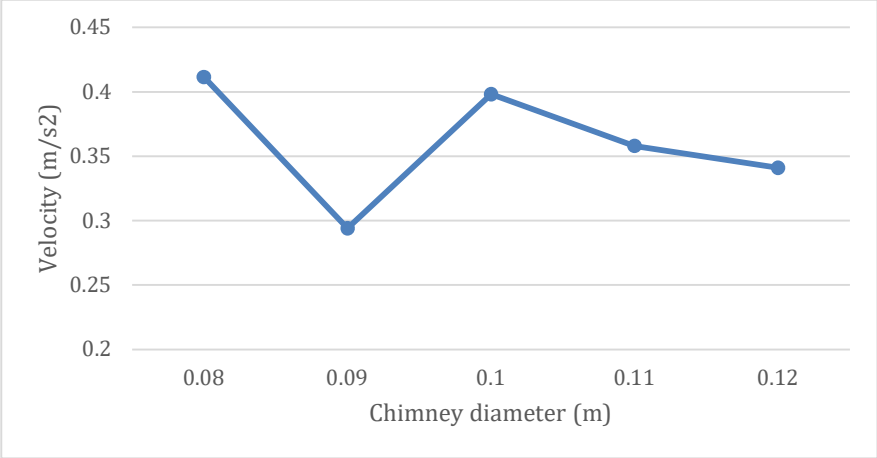


Figure 12. Fluid flow velocity through chimney outlet

The mean velocity within the chimney exhibits a generally decreasing trend as the pipe diameter is increased as shown in figure 12, declining from 0.411 m/s at a diameter of 0.08 m to 0.341 m/s at 0.12 m. This behavior is consistent with the principle of continuity: for a volumetric flow rate of buoyancy-driven combustion gases, enlarging the cross-sectional area of the chimney necessitates a proportional reduction in mean flow velocity. The driving force for this natural convection flow, the thermal buoyancy arising from the density difference between hot flue gases and ambient air, does not scale proportionally

with the chimney cross-section, and therefore the system cannot sustain the same velocity magnitude as the passage widens.

The velocity recorded at 0.09 m diameter deviates from the otherwise general decreasing trend observed across the remaining cases. The cause of this deviation could not be conclusively determined from the present simulation data alone. A mesh independence study targeting this specific case, along with residual convergence monitoring, would be necessary to establish whether this represents a genuine physical phenomenon as other than diameter, all parameters are the same for each case.

4.2.2 Temperature on monitor points

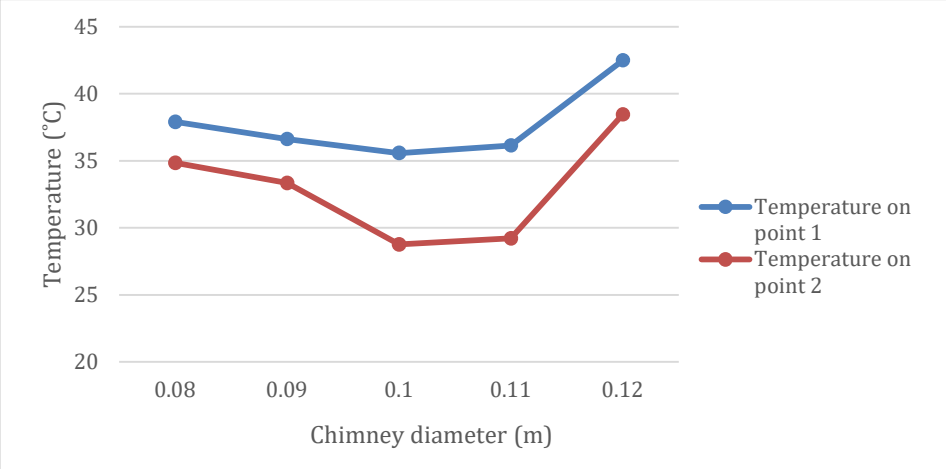


Figure 13. Temperature recorded at monitor points

From figure 13, it is seen that the gas temperatures recorded at the two axial monitor points at the 90-minute mark exhibit a non-monotonic, slight U-shaped trend with respect to chimney diameter. Both measurement locations follow a consistent pattern: temperatures are relatively elevated at the smallest diameter (34.84°C and 37.90°C at points 1 and 2, respectively), decrease to a minimum in the intermediate range (reaching 28.77 °C and 35.58 °C at 0.10 m), and subsequently recover to higher values at the largest diameter (38.46 °C and 42.50 °C at 0.12 m).

At the smallest diameter of 0.08 m, not only does the temperature of monitor points high, but also the outlet velocity of fluid in chimney is the highest. This is a notable point as air escaping at such high velocity would leave no room for the chimney to retain as much heat, but the overall inside temperature is elevated compared to that of intermediate diameter. One possible reason could be attributed to the heat being dissipated through other outlets like heat flux and surface radiation from the stove or heat is being removed through outlet instead. To investigate the second hypothesis, outlet gas temperature is

measured and shown in figure 14. However, it being relatively lower at smaller diameters (0.08m and 0.09m) does not support the idea, but it is consistent with the observation of flow velocity. This suggests that other competing mechanisms are active

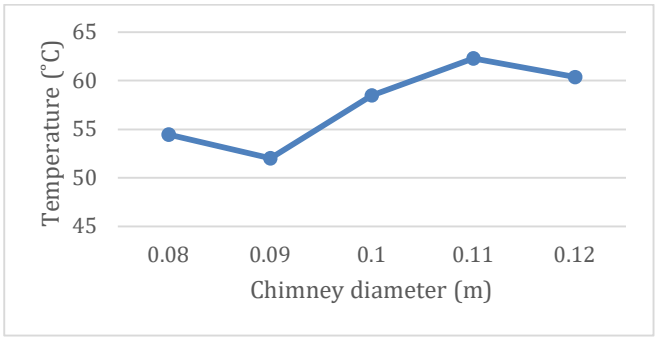


Figure 14. Outlet gas temperature

The monitor points' temperature minimum observed in the 0.09–0.10 m range corresponds to a transitional flow regime in which gas velocity has decreased sufficiently to allow greater convective heat loss to the chimney walls, yet no significant recirculation zones have formed to retain thermal energy near the monitor points. This represents the most aerodynamically efficient configuration in terms of heat extraction along the chimney length.

At the lar*ger* diameters of 0.11 m and 0.12 m, the temperature recovery is attributed to two concurrent mechanisms. First, the reduced flow velocity allows the development of recirculation zones within the wider chimney bore, trapping pockets of hot gas in the vicinity of the monitor points and elevating local temperatures. Second, the simultaneous increase in stove surface heat flux at 0.12 m (discussed further in Section 4.3) indicates an intensification of combustion, which supplies hotter gases to the chimney inlet. The interaction of these two effects produces the secondary temperature rise observed at the upper end of the diameter range.

4.2.3 Radiation heat flux from the stove surface

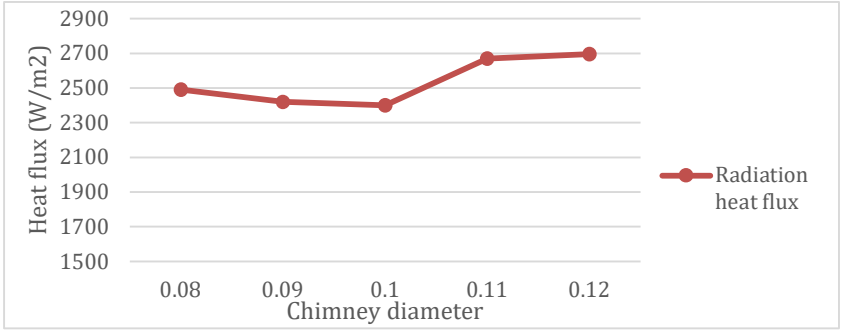


Figure 15. Surface and radiation heat flux from the stove

The radiative heat flux from the stove wall follows a pattern broadly similar to the monitor point temperatures, exhibiting a decreasing trend from 2490.9 W/m² at 0.08 m to a minimum of 2400.3 W/m² at 0.10 m, followed by a recovery to 2696.3 W/m² at 0.12 m. Radiation from a solid surface is governed by the absolute surface temperature raised to the fourth power, meaning that even modest changes in stove wall temperature produce disproportionately large variations in radiative output.

At the smaller diameters, inside temperature elevation has a slight potential to be explained by the radiation flux emitted from the stove. Even though the velocity is higher, the volume of gas removed per second is lower (0.00827m/s^3 for 0.08m diameter but 0.0154 m/s^3 for 0.12m diameter), indicating that heat is getting trapped in the stove which is proven by the generally high radiation flux for smaller diameter.

For the practical heating performance of the Mongolian *ger*, radiative heat flux from the stove wall is a critical parameter, as it constitutes the primary mechanism by which the occupants experience radiant warmth from the heating appliance. The results suggest that a chimney diameter of 0.12 m produces the highest radiative output; however, this must be balanced against the reduced draft velocity, which may impair flue gas evacuation and increase indoor air pollution risk — a trade-off that warrants further investigation in the context of occupant health and thermal comfort.

4.2.4 Chimney wall heat flux

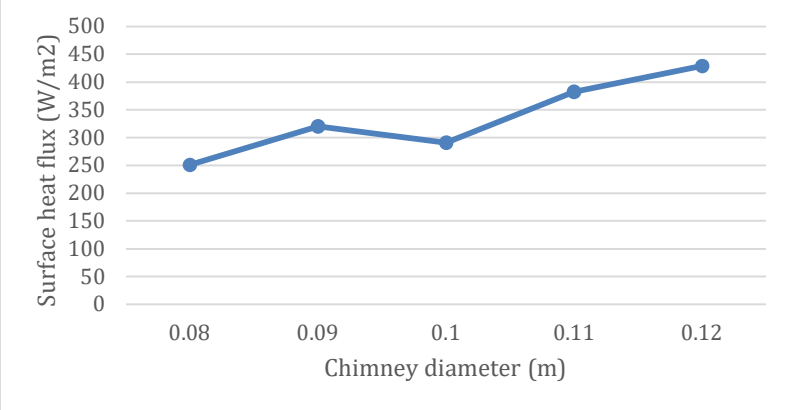


Figure 16. Average chimney surface heat flux

The convective heat flux through the chimney wall displays a clear and consistent increasing trend with chimney diameter, rising from 251.0 W/m² at 0.08 m to 429.3 W/m² at 0.12 m (figure 16). This trend is primarily governed by two competing factors: the increase in wall surface area and the reduction in flow velocity.

As the chimney diameter increases, the total inner surface area available for convective heat transfer grows proportionally. Even where the local convective heat transfer

coefficient may decrease due to lower velocities and a more laminar flow character, the net effect of greater surface area dominates, resulting in higher total wall heat flux. The corresponding increase in average chimney wall temperature, from 85.16 °C at 0.08 m to 90.47 °C at 0.12 m, further proves this interpretation, as the wall temperature elevation is consistent with prolonged thermal contact between the slower-moving gas and the pipe wall.

4.3 Influence of Varying Number of Annular Fins

This section presents and discusses the results of four simulations in which the number of external annular fins mounted horizontally on the outer surface of the chimney pipe was varied from zero to nine, while all other parameters — including chimney diameter (0.10 m), pipe length (2.0 m), wall thickness (0.002 m), and heat generation — were held constant. Each fin consists of a steel disk of the same material and thickness as the chimney wall (0.002 m), with an inner radius matching the chimney outer radius and extending 0.03 m radially outward, distributed equally along the chimney height. While the comparison figures are shown in Appendix B, the results are summarized in Table C2 in Appendix C, which includes derived values of total dissipating surface area and total heat transfer rate computed from the reported average heat flux and the combined chimney wall and fin surface area for each configuration.

4.2.1 Total Surface Heat Flux and Heat Transfer Rate

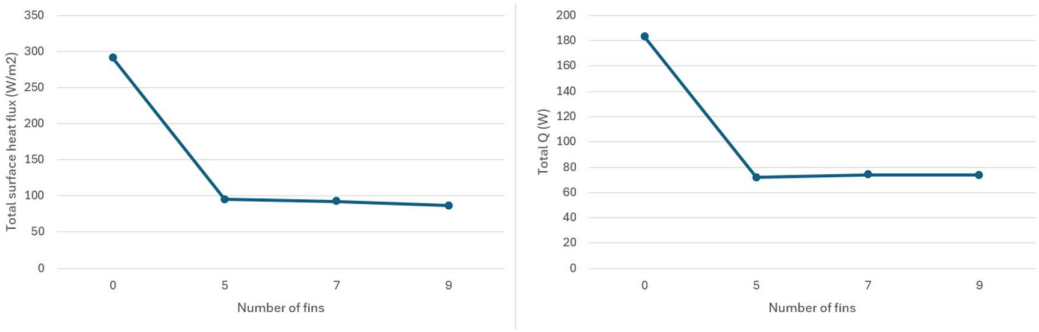


Figure 17. Total surface heat flux and heat transfer rate of stove walls

A direct comparison of the reported average heat flux values across fin configurations would suggest a monotonically decreasing trend (Figure 17), from 291.15 W/m² in the no-fin baseline to 86.50 W/m² at nine fins. However, this interpretation is misleading without accounting for the fact that the average flux is computed over an increasing total surface area as fins are added. As each annular fin contributes an additional 0.0255 m² of dissipating surface, the denominator of the area-averaged heat flux grows substantially with each configuration, compressing the reported value even if the total energy dissipated remains constant or increases.

To obtain a physically meaningful comparison, the total heat transfer rate was computed by multiplying the reported average flux by the corresponding total surface area for each case. The results reveal a finding of considerable significance: the no-fin baseline configuration transfers approximately 182.9 W, whereas all finned configurations transfer only 71.9 to 74.1 W; a reduction of approximately 60 percent relative to the baseline. This outcome is contrary to the conventional expectation that external fins enhance heat transfer, and warrants a detailed physical explanation rooted in the specific geometry of horizontal annular fins on a natural convection system.

The orientation of the fins is central to understanding the degraded thermal performance. Unlike longitudinal fins which run parallel to the chimney axis and permit buoyancy-driven air to rise freely along the chimney surface, horizontal annular fins are oriented perpendicular to the direction of natural convection. Each disk fin acts as a physical baffle that the rising warm air around the chimney exterior must navigate around rather than along. This fundamentally disrupts the boundary layer development on the outer chimney surface by repeatedly interrupting the rising air column at each fin location, preventing the continuous development of a convective boundary layer that would otherwise carry heat efficiently away from the pipe.

Furthermore, the air entrapped between adjacent horizontal disk fins occupies a semi-enclosed cavity bounded above and below by fin surfaces and laterally by the chimney wall. Within this inter-fin space, the buoyancy-driven circulation is constrained, and the air can approach thermal saturation, reaching a temperature close to that of the surrounding surfaces, thereby drastically reducing the effective temperature difference driving convection within these cavities. This stagnation effect becomes more pronounced as the number of fins increases and the inter-fin spacing decreases, which is consistent with the observed plateau in total heat transfer between seven and nine fins and the continued decline in average heat flux per unit area.

4.2.2 Chimney Wall Temperature and Draft Suppression

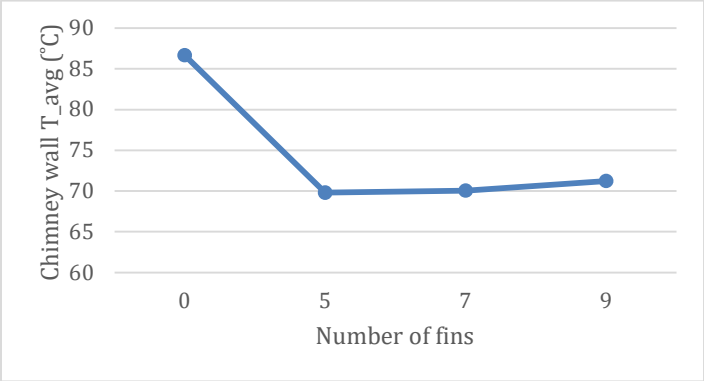


Figure 18.Chimney Wall Temperature

From Figure 18, the introduction of annular fins produces a sharp reduction in average chimney wall temperature, falling from 86.66°C in the no-fin case to approximately 69.7°C with five fins, remaining near this level across all finned configurations. This reduction corresponds to a decrease in the temperature difference between the chimney surface and the *ger* interior ambient from approximately 61.7°C to 44.7°C, a drop of roughly 27 percent. Since natural convective heat transfer from the chimney exterior is directly proportional to this driving temperature difference, the effective convective output of the chimney surface is substantially weakened in all finned cases despite the increased surface area.

This wall temperature depression is a direct consequence of the annular fins conducting heat radially outward from the chimney wall. While this initially appears beneficial, the cooler chimney wall produces a weaker buoyancy-driven draft within the *ger* interior, which in turn reduces the velocity of hot flue gases flowing through the chimney interior. Outlet velocity drops from 0.398 m/s in the baseline to between 0.282 and 0.338 m/s across finned cases, a reduction of 15 to 29 percent (Figure 19). The slower internal flow delivers thermal energy from the combustion chamber to the chimney walls at a reduced rate, diminishing the heat available for external transfer regardless of the fin area present.

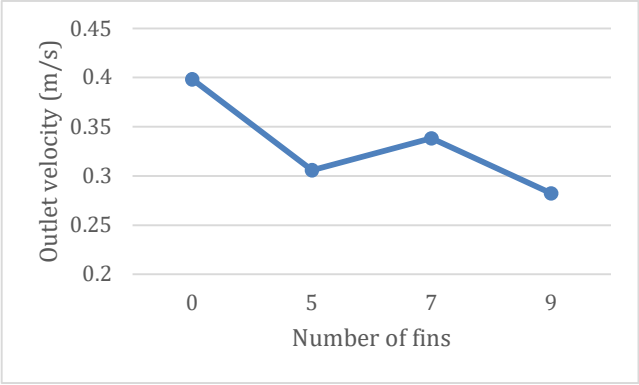


Figure 19. Outlet velocity trend

This constitutes a coupled thermal-fluid feedback loop specific to natural convection systems: external fin cooling depresses wall temperature, which weakens the buoyancy draft, which reduces internal convection, which further reduces the wall temperature. This feedback is absent from classical extended surface analysis, which treats the fin base temperature as a fixed boundary condition independent of the flow field. In the present system, the base temperature of each annular fin is dynamically coupled to the internal flow, making the standard fin efficiency framework insufficient to predict system-level behavior without accounting for this interaction.

4.2.3 Monitor Point Temperatures and Internal Gas Behavior

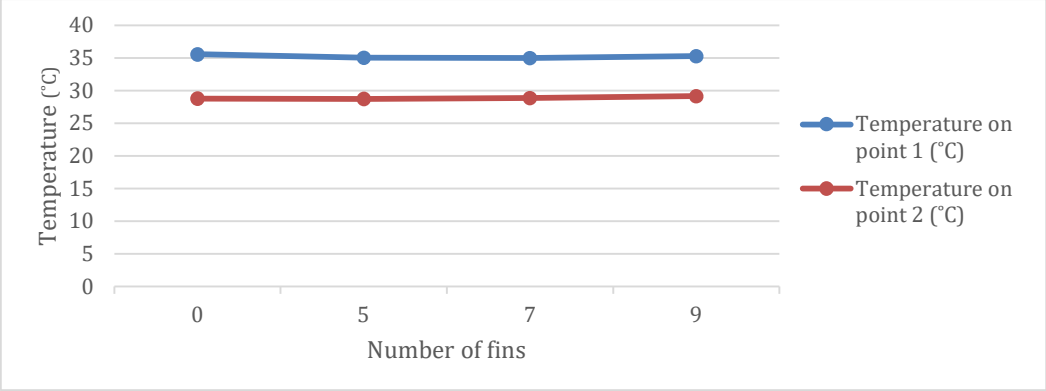


Figure 20. Monitor point temperatures

The temperatures at the two internal monitor points remain essentially stable across all fin configurations, ranging from 34.99 to 35.58°C at point 1 and from 28.72 to 29.15°C at point 2. This near invariance confirms that the internal bulk gas temperature is governed primarily by the fixed heat input from the stove rather than by the external thermal boundary conditions imposed by the fins. The slight upward drift in point 2 temperature with increasing fin number may reflect mild recirculation intensification near the upper chimney region as the weakening draft allows marginally warmer gas to lin*ger* near the measurement location. The overall stability of monitor point temperatures across configurations confirms that the observed differences in system thermal performance are attributable entirely to changes in the external dissipation pathway and the consequent feedback on internal draft velocity, rather than to any modification of the heat source behavior.

4.2.4 Stove Surface Heat Flux Response

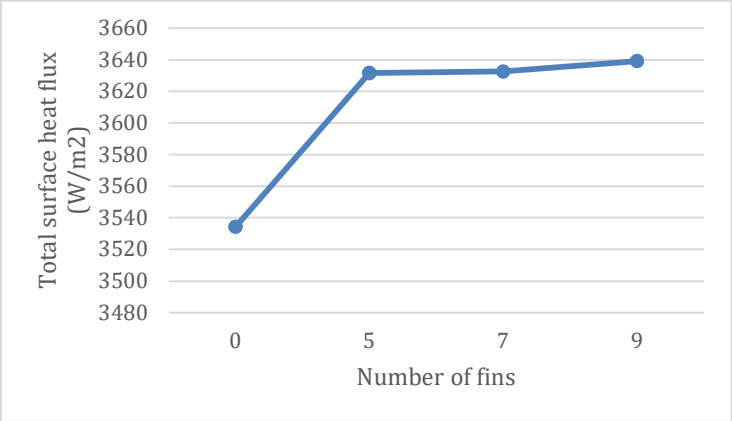


Figure 21. Total surface heat flux from stove walls

The stove surface heat flux increases modestly but consistently with fin number, from 3534.3 W/m² in the baseline to 3639.1 W/m² at nine fins — an increase of approximately 105 W/m² or 3 percent. Since heat generation is constant across all cases, this increase reflects the altered convective boundary conditions at the stove wall induced by the weakened chimney draft. With slower flue gas movement, hot gases are drawn away from the stove surface less rapidly, marginally elevating the local gas temperature adjacent to the stove wall. This reduces convective cooling of the stove surface, which under fixed heat generation manifests as a higher computed surface heat flux as the wall temperature adjusts to maintain thermal equilibrium. This response is consistent with and further corroborates the draft suppression mechanism identified in Section 4.2.2.

Among the three finned cases, total heat transfer rates are effectively indistinguishable: 71.9 W at five fins, 74.1 W at seven fins, and 73.7 W at nine fins. This saturation indicates that beyond five fins, the incremental surface area contributed by additional annular disks yields no meaningful improvement in total heat output. Two mechanisms are responsible. First, as the number of horizontal disk fins increases, inter-fin spacing decreases, deepening the stagnation effect within the enclosed cavities between adjacent fins and progressively reducing the convective coefficient on the fin faces. Second, the aerodynamic obstruction imposed on external natural convection worsens with each additional disk, further limiting the entrainment of ambient air around the chimney. The net result is that the thermal benefit of additional surface area is entirely offset by the worsening flow obstruction and inter-fin air stagnation.

The results demonstrate that horizontal annular fins in their current configuration are counterproductive for the Mongolian *ger* chimney application, reducing total heat dissipation by approximately 60 percent relative to the un-finned baseline. The dominant

cause are possibly the fin's thickness being "paper-thin" and the perpendicular orientation of the fins relative to the natural convection flow direction, which simultaneously obstructs buoyancy-driven air circulation around the chimney exterior and suppresses the internal draft through the coupled wall temperature feedback described above. These findings suggest that if external fins are to be incorporated into *ger* chimney design, vertical or inclined fin orientations that align with rather than oppose the natural convection flow direction should be considered. Additionally, optimization of inter-fin spacing to prevent air stagnation and selection of fin dimensions that limit wall temperature depression while maximizing effective heat transfer area would be necessary prerequisites for achieving a net thermal benefit. Experimental validation under realistic operating conditions would be essential to confirm any computationally derived optimum configuration.

4.3 Influence of Coaxial cylindrical extension

This section presents and discusses the results of three simulations in which the base chimney configuration (diameter 0.10 m, height 2.0 m) was progressively fitted with a coaxial cylindrical steel extension at its lower end. The extension was modelled as a closed steel cylinder of the same thickness and material as the chimney pipe (2 mm thick steel), with an inner diameter matching the chimney pipe at the top outlet and a sealed bottom plate with a central inlet opening for flue gas inlet. Extension diameters of 0.2 m and 0.25 m were simulated, both with a fixed height of 0.816 m approximated from the dimensional descriptions available in Stehr et al. (2025). All other simulation parameters, including heat generation, remained constant across cases. The results are summarized in Table C3, which includes derived total surface areas and total convective heat transfer rates. Models designed are also available in Appendix B.

4.3.1 Total heat transfer derivation from surface area

As with the fin variation study in Section 4.2, the reported average heat flux values cannot be compared directly across configurations without accounting for the substantial increase in total dissipating surface area introduced by the extension. The 0.2 m extension adds an outer cylindrical wall of 1.020 m^2, two annular end plates totaling 0.047 m^2, and retains the full 0.373 m^2 chimney outer wall, yielding a total surface area of 1.441 m^2. The 0.25 m extension produces a total area of 1.731 m^2. In contrast, the baseline chimney presents only 0.628 m^2 to the *ger* interior.

When total heat transfer rate is derived by multiplying the average flux by the corresponding total surface area, the results reveal a considerably more nuanced picture than the raw flux values suggest. The 0.2 m extension achieves a total

convective output of approximately 213.8 W, an increase of 16.9 percent over the baseline value of 182.9 W. This is a genuinely positive result: the extension successfully augments net convective heat delivery to the *ger* interior, demonstrating that the additional surface area it introduces more than compensates for the reduction in average flux caused by the lower wall temperature and weakened draft. The 0.25 m extension, however, produces approximately 129.8 W, a reduction of 29.0 percent from the baseline, indicating that at this larger diameter the thermal penalty of draft suppression and wall temperature depression overtakes the benefit of the increased surface area, reversing the performance advantage seen at 0.2 m. This non-monotonic behavior, where an intermediate geometry outperforms both the baseline and the larger configuration, is the central finding of this parametric study and is discussed further in subsequent sections.

4.3.2 Chimney wall temperature

A consistent and physically coherent pattern is observed in the average chimney wall temperature across the three configurations: 86.66°C at baseline, 73.30°C at 0.2 m extension, and 67.14°C at 0.25 m extension. This progressive decline with increasing extension diameter follows the same coupled thermal-fluid mechanism identified in the fin variation study and is rooted in the interaction between external surface area, wall temperature, and internal draft strength.

The extension encloses a wider cylindrical volume around the lower chimney section through which flue gas must expand before being directed upward into the narrower chimney bore. This expansion reduces the local flow velocity within the extension chamber, increasing gas residence time in that region and promoting greater heat transfer to the extension walls. While this initially appears beneficial, the consequence is that the extension walls, and by conduction the chimney wall, operate at a lower average temperature than in the unextended case. The cooler wall surface generates a weaker buoyancy-driven draft, which in turn reduces the rate at which hot flue gases are drawn from the combustion chamber. This is directly reflected in the outlet velocity data: velocity falls from 0.398 m/s at baseline to 0.318 m/s at 0.2 m and 0.302 m/s at 0.25 m, reductions of 20 and 24 percent respectively. The draft suppression mechanism thus operates in the extension geometry through the same fundamental feedback loop described in Section 4.2.2, wherein external heat dissipation, wall temperature depression, and internal velocity reduction are mutually reinforcing effects.

4.3.3 Stove Total Surface Heat Flux

The stove surface heat flux increases progressively with extension diameter, from 3534.3 W/m^2 at baseline to 3572.5 W/m^2 at 0.2 m and 3627.8 W/m^2 at 0.25 m, consistent with weakening draft reducing convective cooling at the stove wall under constant heat generation. The average stove wall temperature correspondingly rises, but only marginally: from 230.77°C at baseline to 231.64°C at 0.2 m and 232.56°C at 0.25 m, a total increase of only 1.79°C across the full range. Applying Stefan-Boltzmann scaling to these absolute temperatures predicts a radiation increase of approximately 0.7 percent at 0.2 m and 1.4 percent at 0.25 m relative to the baseline.

The actual radiation flux data, however, departs dramatically from this prediction at the 0.25 m configuration. At 0.2 m, the measured radiation of 2429.8 W/m^2, a 1.2 percent increase, is broadly consistent with the temperature-based expectation. At 0.25 m, however, the measured radiation of 2845.4 W/m^2 represents an 18.5 percent increase over the baseline, compared to the 1.4 percent predicted from the average wall temperature alone. This discrepancy of more than an order of magnitude cannot be attributed to the bulk stove wall temperature change, which is negligible. The monitor point temperatures further reinforce this, point 2 temperatures at 0.2 m and 0.25 m are virtually identical (shown in Table 6), confirming that the bulk flue gas thermal state is nearly the same in both extended configurations and cannot account for the radiation divergence between them.

Table 6. Temperatures recorded at two monitor points for cylindrical extension cases

Chimney extension diameter	Temperature on point 1 ($^{\circ}C$)	Temperature on point 2 ($^{\circ}C$)
No extension	35.58	28.77
0.20m	33.91	25.66
0.25m	33.48	25.65

The most plausible explanation is that the 0.25 m extension geometry induces a localized redistribution of the near-wall flow field at the stove-extension interface that is not reflected in area-averaged quantities. The wider chamber may produce a recirculation zone or stagnation region adjacent to specific portions of the stove wall, locally suppressing convective heat removal from those surface patches and allowing them to reach temperatures substantially higher than the area-averaged wall temperature suggests. Since radiation is governed by local surface temperature rather than its average, even a relatively small high-temperature zone can dominate the total radiative output if its temperature is sufficiently elevated. This interpretation is consistent with the

observation that the average wall temperature increases by only 1.79°C while radiation rises by 18.5 percent; a response that is physically coherent only if the temperature distribution across the stove wall is becoming increasingly non-uniform as the extension diameter grows. Confirmation of this hypothesis would require local surface temperature mapping or a spatially resolved post-processing of the stove wall heat flux distribution.

4.4 Comparison between annular fin variation and cylindrical extension variation

Comparing the extension geometry results with those of the fin variation study reveals both similarities and important distinctions. Both modifications share the same root mechanism: additional external steel surface area depresses the chimney wall temperature, weakens the internal draft, and reduces total convective heat output relative to the unmodified baseline. However, the magnitude and consequence of this effect differ substantially between the two geometries.

In the fin variation study, all finned configurations reduced total convective output by approximately 60 percent, with no compensating benefit in radiation, the stove radiation increased by only 3 percent. The extension geometry, by contrast, produces a far more moderate convective reduction at 0.2 m (3.6 percent) and a dramatically larger radiation enhancement at 0.25 m (18.5 percent). This difference in radiation response is attributable to the greater flow restriction imposed by the expansion-contraction geometry of the extension, which more severely suppresses draft and allows stove wall temperature to rise more substantially than the fin geometry could produce.

From a practical design perspective, the 0.2 m extension emerges as the most balanced configuration examined in this study. It maintains near-baseline convective heat transfer while adding significant additional radiating surface area to the lower chimney zone — a region of the *ger* interior that is typically proximate to occupants. The 0.25 m extension, while producing notable radiation enhancement, incurs too large a convective penalty to be recommended without further optimization. Both configurations would benefit from experimental validation under real operating conditions.

5 Limitations

While the numerical models developed in this study aim to replicate the essential thermal and fluid dynamic behavior of the *ger* interior, simplifications applied across each aspect of this study introduce limitations that must be acknowledged when interpreting the results.

First, the models assume perfect geometric symmetry, treating the *ger* wall as an idealized converging cylinder and empty. Asymmetric features and furniture inside would change how fluid flows and heat dissipates. Only annular fins are investigated in this thesis and came to be highly inefficient form of modification. The axisymmetric modelling approach did not allow longitudinal fins to be investigated. Also even though validated through other means of verification, residual plots show that continuity is above the accepted threshold.

Second, the fluid medium is modelled under the Boussinesq approximation, which assumes that density variations due to temperature differences are small enough to be treated as a buoyancy term only. This approximation becomes less accurate at large temperature gradients, which are plausible near the stove surface during transient heating. Furthermore, wind-induced infiltration through the *ger* fabric is neglected entirely, despite being a potentially significant source of heat loss and air movement under real outdoor winter conditions.

Third, the radiative heat transfer model treats the interior air as an optically thin, weakly participating medium with absorption and scattering coefficients chosen by trial and error to match experimental data. While the resulting optical thickness confirms the optically thin assumption, the selected values remain approximate.

Fourth, the thermal boundary conditions applied to the *ger* envelope represent a substantial simplification. The multilayer structure of the actual *ger* wall, comprising wood lattice, multiple felt layers, and additional insulating materials, is reduced to an equivalent wood layer characterized by a single heat transfer coefficient. This simplification may introduce error in the predicted rate of heat loss through the envelope, particularly given that the thermal resistance of the real wall is both higher and more variable than the model assumes.

Finally, and most importantly, the model is validated against a single experimental dataset from one measurement period reported by Purev et al. (1), covering a specific *ger* under specific outdoor conditions. Consequently, the degree to which the calibrated

parameters generalize to other *ger* geometries, stove outputs, or ambient temperatures remains uncertain. These limitations collectively mean that the absolute temperature and velocity values predicted by the simulations should be interpreted with caution, even though the comparative conclusions drawn between model configurations remain valid within the scope of this study.

6 Conclusion

This thesis has conducted the first numerical investigation into how chimney geometry affects heat transfer performance in the Mongolian traditional *ger* heating system. Using ten transient CFD simulations validated against published experimental data, three categories of geometric modification were evaluated: variation of chimney inner diameter, addition of external horizontal annular fins, and installation of coaxial cylindrical extension.

The diameter study revealed that the relationship between chimney inner diameter and indoor thermal performance is not monotonic. Indoor temperatures at both monitoring locations followed a U-shaped trend, reaching a minimum at the current MASM-standard diameter of 0.10 m. This finding suggests that the standard diameter may not represent the thermally optimal configuration, and that larger diameters, particularly 0.12 m, may deliver higher radiative heat flux from the stove surface, although at the cost of reduced draft velocity. The trade-off between draft strength and heat retention is a fundamental design tension that any chimney geometry optimization must address.

The annular fin study produced the most counterintuitive result of the thesis. Contrary to the conventional expectation that external fins enhance heat transfer by increasing dissipating surface area, all finned configurations reduced total heat transfer by approximately 60% relative to the bare cylinder baseline. The horizontal orientation of the fins proved to be fundamentally incompatible with natural convection: the disk fins acted as baffles that interrupted the rising air column along the chimney exterior, caused stagnation in inter-fin cavities, and depressed chimney wall temperature through coupled thermal-fluid feedback that weakened internal draft. These findings demonstrate that horizontal annular fins are counterproductive for *ger* chimneys under natural convection conditions and should not be used in their current form. If fins are to be incorporated in future designs, vertically or obliquely oriented configurations that align with the natural convection flow direction would be required, alongside optimization of inter-fin spacing to prevent thermal stagnation.

The coaxial cylindrical extension study identified an intermediate geometry, the 0.2 m diameter extension, as the most promising configuration examined in this thesis. This geometry achieved a 16.9% increase in total convective heat output over the baseline, demonstrating that additional dissipating surface area introduced by the outer cylinder can more than compensate for the draft suppression it induces, provided the extension diameter is not too large. The 0.25 m extension, by contrast, produced a 29.0% reduction in convective output and an anomalously large 18.5% increase in stove surface radiation, likely attributable to localized flow stagnation near the stove wall creating spatially non-uniform surface temperatures. From a practical standpoint, the 0.2 m extension offers a concrete, installable modification to existing *ger* chimneys that could meaningfully increase heat delivered to the living space, and its geometry is directly compatible with the electrostatic dust precipitator design previously field-tested in Ulaanbaatar (8).

Overall, the 0.2 m coaxial cylindrical extension emerges as the configuration that best satisfies the combined requirements of enhanced heat transfer and acceptable draft performance among those studied. The bare chimney at 0.12 m diameter represents the second-best option for occupants prioritizing radiant warmth from the stove surface. Horizontal annular fins in their current configuration are not recommended.

Several limitations must be acknowledged. The two-dimensional axisymmetric model necessarily omits asymmetric features of real *ger* interiors, including furniture, door placement, and non-uniform envelope materials. The Boussinesq approximation introduces potential inaccuracy near the high-temperature stove surface. The model is validated against a single experimental dataset from one *ger* under specific outdoor conditions, and the degree to which the calibrated parameters generalize to other configurations remains uncertain. Additionally, the continuity residual did not meet the conventional convergence threshold, although all other residuals converged satisfactorily and the physical sanity checks and reference comparison support the validity of the results.

Future work should extend the investigation to 3D models capable of capturing asymmetric flow patterns, consider especially fin geometries including vertically oriented fins, and validate computational predictions experimentally under real winter operating conditions. Parametric studies combining geometric optimization with indoor air quality metrics, particularly carbon monoxide concentration, would provide a more holistic basis for design recommendations that address both the heating efficiency and health dimensions of *ger* stove system performance.

7 References

1. Uelun-Ujin Purev AHMB. Indoor thermal environment of Mongolian traditional mobile housing used as urban habitat in winter. Journal of building engineering. 2022 May; 48: 103927.
2. Tsovoodavaa G SRBMKI. A review and systemization of the traditional Mongolian yurt (GER). Pollack Periodica. 2018 Dec;: 19–30.
3. Kemery B. Yurts: Living in the round. First Edition ed. Layton: Gibbs Smith; 2006.
4. Mrkonjic K. Autonomous Lightweight Houses: Learning from Yurts. In the 23rd Conference on Passive and Low Energy Architecture; 2006; Geneva.
5. Bat-Erdene B YUAA. Experimental Investigation and Energy Performance Simulation of Mongolian Ger with ETS Heater and Solar PV in Ulaanbaatar City. Energies. 2020 Nov; 13: 5840.
6. Myeong-Seon Chae BJC. Heat transfer effects of chimney height, diameter, and Prandtl number. International Communications in Heat and Mass Transfer. 2015 Aug; 66: 196-202.
7. Byambakhorol Battsetseg GGBN. Measurement and 3-dimensional Simulations of Carbon Monoxide (CO) Distribution in Mongolian Ger. In Advances in Engineering Research; 2023. p. 117-131.
8. Stehr GC KDBBSL. Pilot-Testing Electrostatic Dust Precipitators in Ulaanbaatar/Mongolia: Insights into Particulate Matter Composition and Potential for Air Pollution Reduction. In Advances in Engineering Research; 2025. p. 143–162.
9. Erdenedavaa P AAAAOE. Performance analysis of solar thermal system for heating of a detached house in harsh cold region of Mongolia. Renewable Energy. 2018 Mar; 117: 217-226.
10. Du P HA. Retrofitting strategies for thermal comfort and sustainability in Ulaanbaatar’s traditional housing. Journal of Building Engineering. 2025 May; 11803: 101.
11. William W. Braham MHMBGJJTSE. Cooking, Heating, Insulating Products and Services (CHIPS) for Mongolian ger: Reducing energy, cost, and indoor air pollution. Energy for Sustainable Development. 2022 Dec; 71: 462-479.
12. Nasanjargal B GG. CFD-based Optimization of Stove Designs for Sustainable Heating in Mongolian Gers. Advances in Engineering Research. 2025;: 231-242.
13. Metrology MAfSa. MNS 5216. 2016. Stove for Household. General Technical requirements.
14. Christie WW. Chimney Design and Theory for Engineers and Architects London: D.Van Nostrand Company; 1899.
15. Sriram Chandrashekar VMRKV. Numerical study of buoyant flows in straight and converging chimneys. International Communications in Heat and Mass Transfer. 2022 Jul; 136(106210).
16. W E. The dissipation of heat by free convection the inner surface of vertical tubes of different shapes of cross-section. Physica. 1942 Sep; 9: 865-874.

17. Haaland SE SE. Solutions for the channel plume and the parallel-walled chimney. Numerical Heat Transfer. 1983 Apr; 6: 155-172.
18. Yunus A. Çengel AJG. Heat and mass transfer: Fundamentals and applications. 4th ed. Lange M, editor. New York: Mcgraw-Hill; 2010.
19. Le Fevre EJ. Laminar free convection from a vertical plane surface. In Proceedings of the 9th International Congress on Applied Mechanics ; 1956; 4.
20. John H. Lienhard V JHLI. A Heat Transfer Textbook. 6th ed. Cambridge: Phlogiston Press; 2024.
21. H.F. Nouanégué EB. Heat transfer by convection, conduction and radiation in solar chimney systems for ventilation of dwellings. International Journal of Heat and Fluid Flow. 2009; 30: 150-157.
22. Seung-Min Ohk BJC. Natural convection heat transfer inside an open vertical pipe: Influence of length, diameter and Prandtl number. International Journal of Thermal Sciences. 2017; 115: 54-64.
23. Gyeongg-Uk Kang DSY. Laminar natural convection heat transfer depending on diameters of vertical cylinders with circular cross-section with high Prandtl number. International Journal of Heat and Mass Transfer. 2019; 134: 554-565.
24. Qie Shen DSYXTJXZNZKWZH. Natural convection heat transfer along vertical cylinder heat sinks with longitudinal fins. International Journal of Thermal Sciences. 2015; xxx: 1-8.
25. Jnana Ranjan Senapati SKDSR. Numerical investigation of natural convection heat transfer from vertical cylinder with annular fins. International Journal of Thermal Sciences. 2017; 111: 146-159.
26. E. Hahne DZ. Natural convection heat transfer on finned tubes in air. International Journal of Heat and Mass Transfer. 1994 Mar; 37: 59-63.
27. Kuen Tae Park HJKDKK. Experimental study of natural convection from vertical cylinders with branched fins. Experimental Thermal and Fluid Science. 2014 Apr; 54: 29-37.
28. ANSYS I. Ansys Fluent Theory Guide. Canonsburg:; 2025.
29. Engineering O. [Online]. [cited 2026 Apr. Available from: https://assets.omega.com/pdf/tables_and_graphs/emissivity-table.pdf.
30. Forum AFL. [Online]. [cited 2026. Available from: https://innovationspace.ansys.com/forum/.

APPENDIX A: List of Tables, Figures and Equations

List of Tables

Table 1. Technical standards by MASM (13) 3
Table 2. Boundary conditions for solid parts 15
Table 3. Boundary conditions for fluids 15
Table 4. Contours of key time frames: an example 19
Table 5. Values for mesh quality check 21
Table 6. Temperatures recorded at two monitor points for cylindrical extension cases 34

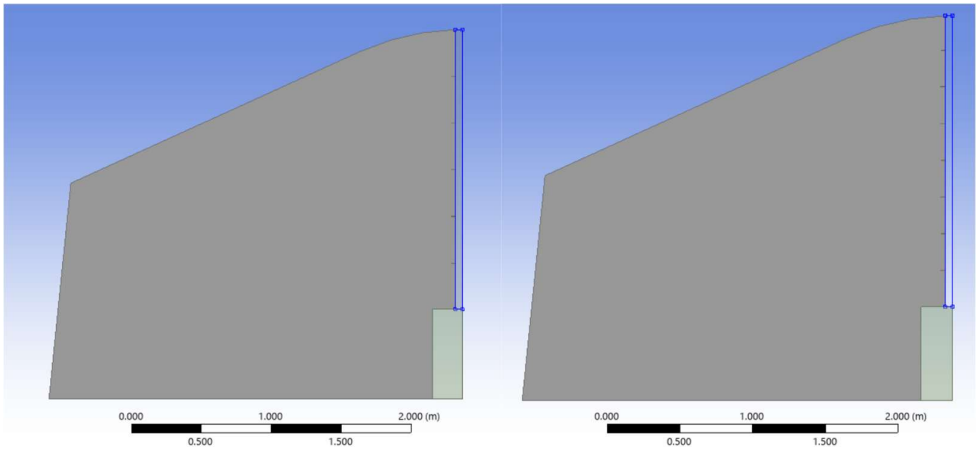
List of Figures

Figure 1. a) Vertical cylinder with longitudinal fins designed by Q. Shen et al. (24) b) Vertical cylinder with annular fins designed by J.R Senapati et al. (25) 9
Figure 2. ESP system's design and state after installation by Stehr et al. (8) 10
Figure 3. The 2D model result after revolution 13
Figure 4. Measurements of ger temperature using coal stove 16
Figure 5. Detailed figure of dimensions by U. -U. Purev et al. 17
Figure 6. 2D model 17
Figure 7. Reference point relative to the ger fluid (locally; x=-0.735m, y=0.5m) 18
Figure 8. Temperature-near-stove against time graph for chimney d=0.1m 18
Figure 9. Residual plot example 20
Figure 10. (a) Coarse mesh (b) Medium mesh (c) Fine mesh used for quality check .. 21
Figure 11. Locations of two monitor points 22
Figure 12. Fluid flow velocity through chimney outlet 23
Figure 13. Temperature recorded at monitor points 24
Figure 14. Outlet gas temperature 25
Figure 15. Surface and radiation heat flux from the stove 25
Figure 16. Average chimney surface heat flux 26
Figure 17. Total surface heat flux and heat transfer rate of stove walls 27
Figure 18.Chimney Wall Temperature 29
Figure 19. Outlet velocity trend 30
Figure 20. Monitor point temperatures 30
Figure 21. Total surface heat flux from stove walls 31

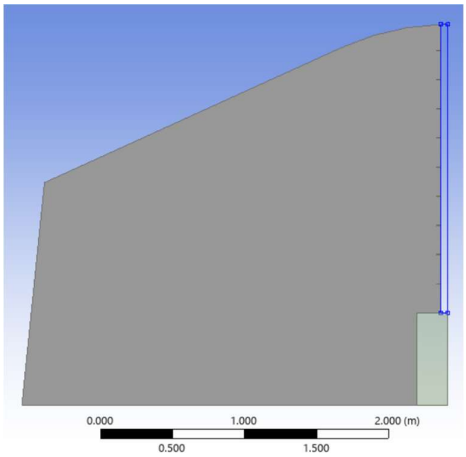
List of Equations

Equation 1 $qrad = \varepsilon\sigma(Ts^4 - T\infty^4)$ 7
Equation 2 $\partial(\rho k)\partial t + \partial(\rho kui)\partial xi = \partial\partial xj\mu\mu t\sigma k\partial k\partial xj + Gk - Yk$ 11
Equation 4 $3\partial(\rho\omega)\partial t + \partial(\rho\omega ui)\partial xi = \partial\partial xj\mu\mu t\sigma\omega\partial\omega\partial xj + G\omega - Y\omega + D\omega$. 11
Equation 4 $\mu t = \rho k\omega \cdot 1max1\alpha * SF2a1\omega$ 12
Equation 5 $\nabla \cdot Ir, ss + a + \sigma sIr, s = an2\sigma T4\pi + \sigma s4\pi 04\pi Ir, s'\Phi s \cdot s'd\Omega'$ 12

APPENDIX B: ***Designs used for the cases of annular fins and cylindrical extension***

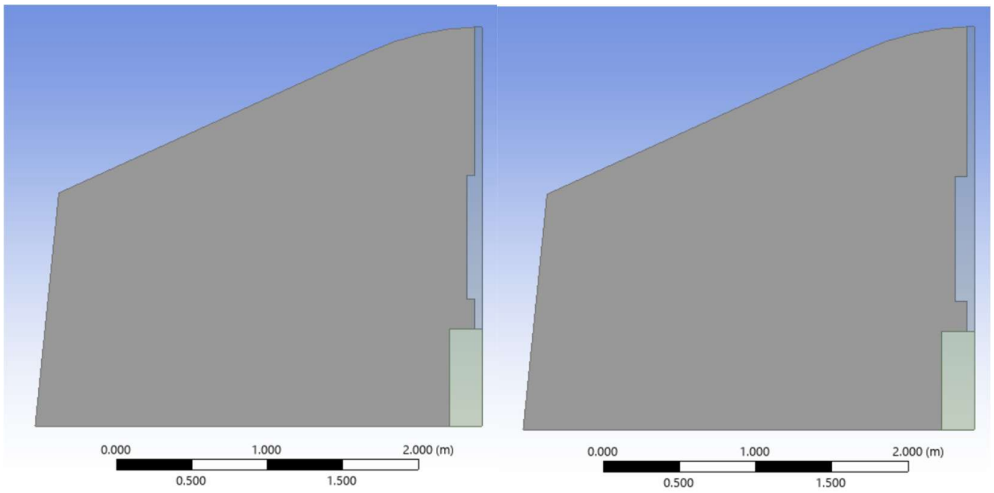


(a)n=5 (b) n=7



(c) n=9

Figure B 1. Designs of annular fin addition



(a)d=0.1m (b) d=0.125m

Figure B 2. Designs of cylindrical extension: two cases

APPENDIX C: Data collected from simulation results

Table C1 Diameter variation

Diameter (m)	Surface area (m^2)	Temperature on point 1 ($^{\circ}C$)	Temperature on point 2 ($^{\circ}C$)	Average value				
				Outlet velocity (m/s)	Chimney wall T_{avg} ($^{\circ}C$)	Heat flux from stove surface (W/m^2)	Heat flux from chimney wall (W/m^2)	Radiation flux from stove wall (W/m^2)
0.08	0.502	37.90	34.84	0.41136	85.156	3576.521	251.0253	2490.865
0.09	0.565	36.63	33.34	0.29396	86.926	3529.041	320.1072	2420.925
0.10	0.627	35.58	28.77	0.39815	86.662	3534.309	291.1528	2400.340
0.11	0.690	36.15	29.22	0.35780	90.448	3451.506	382.2414	2670.701
0.12	0.753	42.50	38.46	0.34084	90.468	3863.332	429.2719	2696.253

Table C2. Fin number variation (Average values)

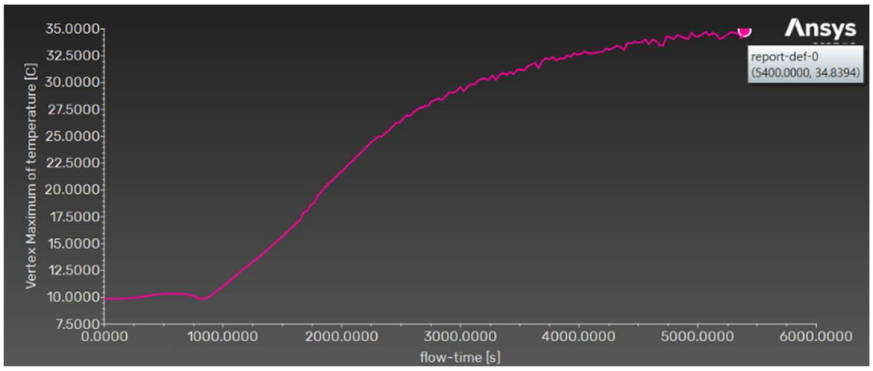
Number of fins	Temperature on point 1 ($^{\circ}C$)	Temperature on point 2 ($^{\circ}C$)	Chimney wall T_{avg} ($^{\circ}C$)	Outlet velocity (m/s)	Heat flux from stove surface (W/m^2)	Heat flux from chimney wall (W/m^2)	Total area (m^2)	Total Q (W)
0	35.58	28.77	86.662	0.39814	3534.309	291.1528	0.628	182.9
5	35.04	28.72	69.7033	0.30586	3631.598	95.5012	0.753	71.9
7	34.99	28.90	70.0481	0.33830	3632.48	92.3903	0.802	74.1
9	35.29	29.15	69.5344	0.28240	3639.127	86.5009	0.852	73.7

Table C3. Coaxial cylindrical extension: two cases

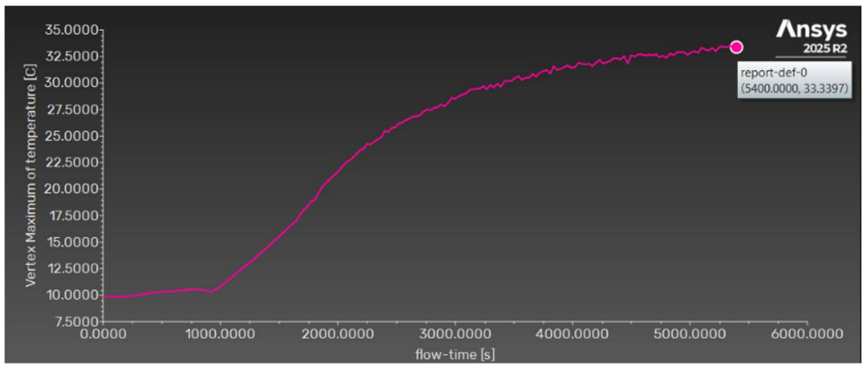
Diameter of extension (m)	Chimney wall T_{avg} ($^{\circ}C$)	Outlet velocity (m/s)	Heat flux from stove surface (W/m^2)	Radiation flux from stove wall (W/m^2)	Heat flux from chimney wall (W/m^2)	Total area (m^2)	Total Q (W)	Stove wall T_{avg} ($^{\circ}C$)
0.1(no extension)	86.662	0.39815	3534.31	2400.34	291.1528	0.628	182.9	230.7749
0.2	73.297	0.31810	3572.49	2429.75	148.4013	1.441	213.8	231.6383
0.25	67.140	0.30199	3627.76	2845.41	74.99084	1.731	129.8	232.5641

APPENDIX D: ***Temperature against time graph for the two monitor points at specified diameter of chimney (Diameter variation case)***

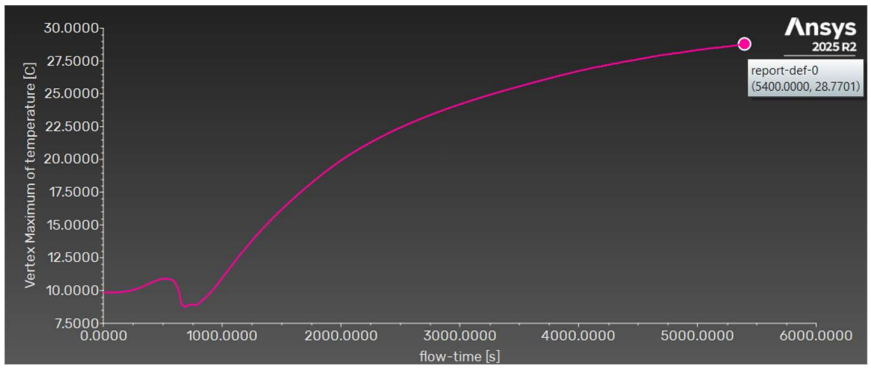
Monitor point 1:



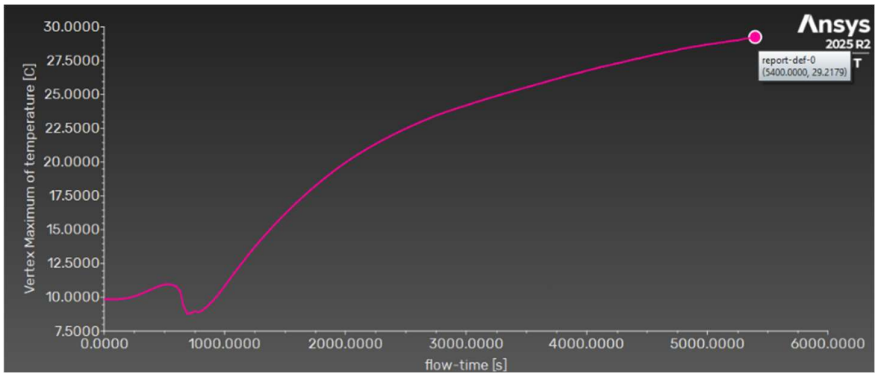
a. d=0.08m



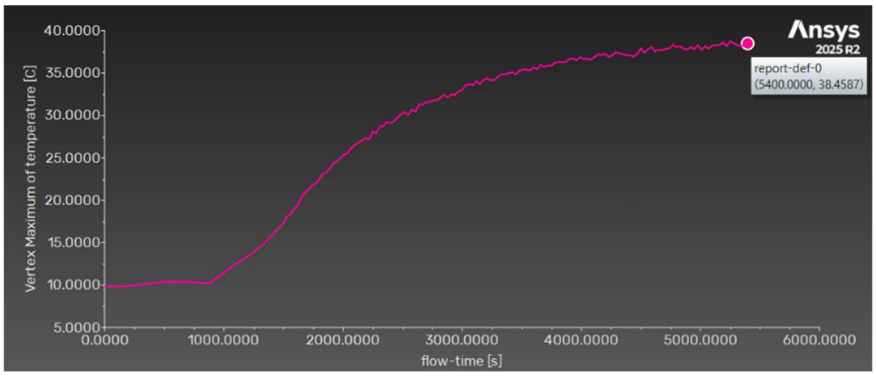
b. d=0.09m



c. d=0.1m

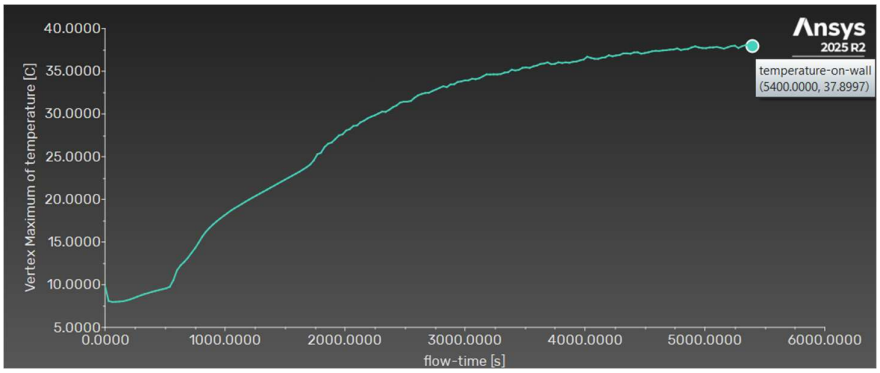


d. d=0.11m

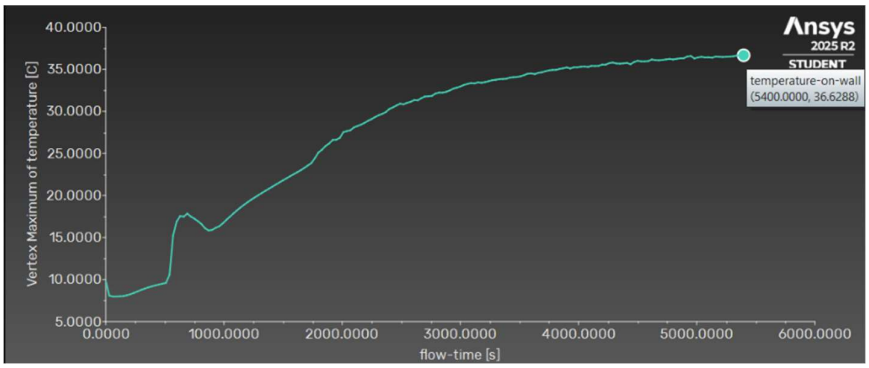


e. d=0.12m

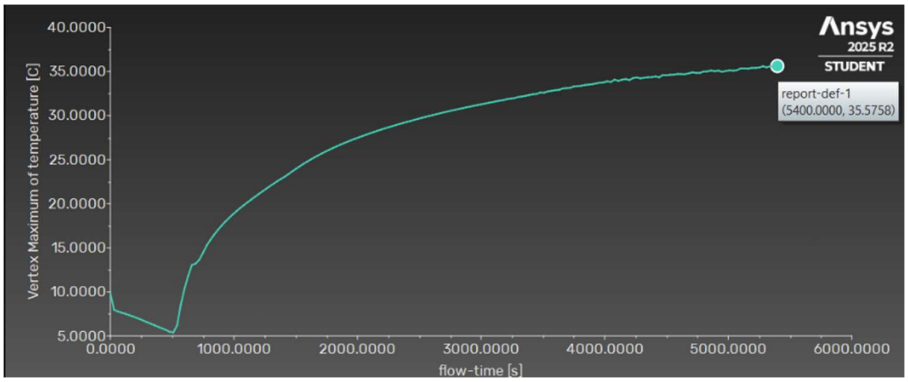
Monitor point 2:



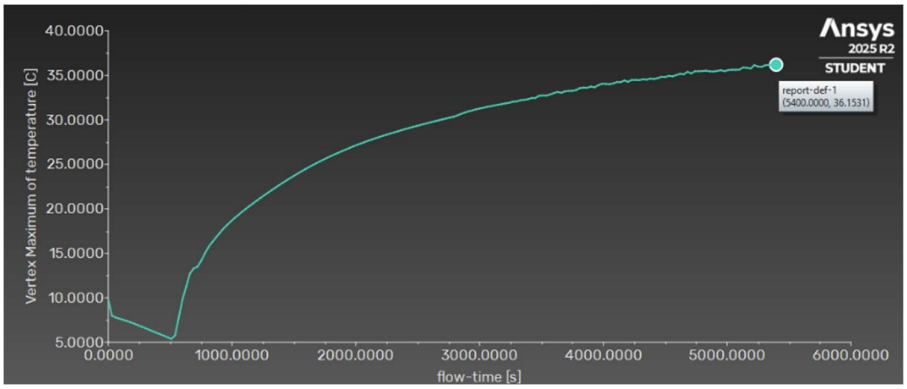
a. d=0.08m



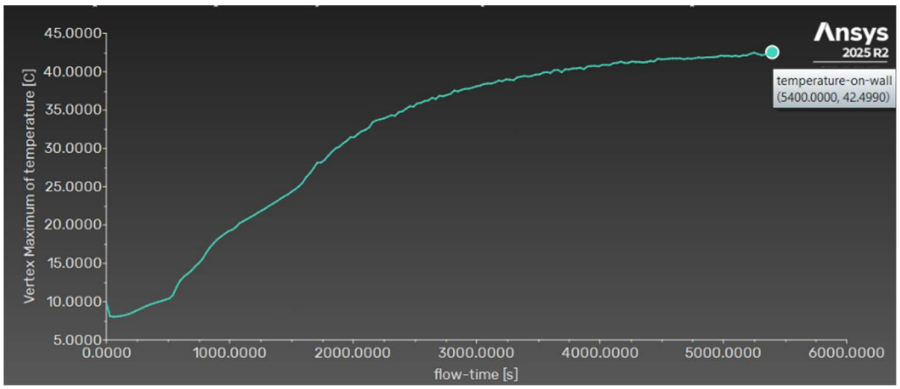
b. d=0.09m



c. d=0.1m



d. d=0.11m



e. d=0.12m